




# Nuclear RNA export factor variant initiates piRNA-guided co-transcriptional silencing

Kensaku Murano<sup>1,†</sup>, Yuka W Iwasaki<sup>1,\*,†</sup> , Hirotsugu Ishizu<sup>1</sup>, Akane Mashiko<sup>1,2</sup>, Aoi Shibuya<sup>1</sup>, Shu Kondo<sup>3</sup>, Shungo Adachi<sup>4</sup>, Saori Suzuki<sup>5</sup>, Kuniaki Saito<sup>3</sup>, Tohru Natsume<sup>4</sup>, Mikiko C Siomi<sup>5</sup>  & Haruhiko Siomi<sup>1,\*\*</sup> 

## Abstract

The PIWI-interacting RNA (piRNA) pathway preserves genomic integrity by repressing transposable elements (TEs) in animal germ cells. Among PIWI-clade proteins in *Drosophila*, Piwi transcriptionally silences its targets through interactions with cofactors, including Panoramix (Panx) and forms heterochromatin characterized by H3K9me3 and H1. Here, we identified Nxf2, a nuclear RNA export factor (NXF) variant, as a protein that forms complexes with Piwi, Panx, and p15. Panx–Nxf2–P15 complex formation is necessary in the silencing by stabilizing protein levels of Nxf2 and Panx. Notably, ectopic targeting of Nxf2 initiates co-transcriptional repression of the target reporter in a manner independent of H3K9me3 marks or H1. However, continuous silencing requires HP1a and H1. In addition, Nxf2 directly interacts with target TE transcripts in a Piwi-dependent manner. These findings suggest a model in which the Panx–Nxf2–P15 complex enforces the association of Piwi with target transcripts to trigger co-transcriptional repression, prior to heterochromatin formation in the nuclear piRNA pathway. Our results provide an unexpected connection between an NXF variant and small RNA-mediated co-transcriptional silencing.

**Keywords** heterochromatin formation; nuclear RNA export factor; RNA silencing; transcriptional regulation; transposable element

**Subject Categories** Chromatin, Transcription & Genomics; RNA Biology

**DOI** 10.15252/embj.2019102870 | Received 5 July 2019 | Revised 10 July 2019 |

Accepted 11 July 2019 | Published online 1 August 2019

**The EMBO Journal (2019) 38: e102870**

## Introduction

Transposable elements (TEs) act as endogenous mobile mutagens to alter the sequence and structure of the genome, thereby changing the transcriptome and chromatin structure. TEs are often deleterious

to the host by, for example, disrupting a gene, but may also be adaptive and drive genome evolution (Han & Boeke, 2005; Chuong *et al*, 2017). TEs comprise nearly half of the human genome and approximately 30% of the genome of *Drosophila melanogaster*; thus, the successively arising families of TEs are the main drivers of genome expansion. In metazoans, TEs are silenced by the piRNA pathway, in which Piwi proteins are guided by Piwi-interacting RNAs (piRNAs) to their targets (Iwasaki *et al*, 2015; Ernst *et al*, 2017). The piRNA pathway is also essential for germline development and fertility in animals (Lin & Spradling, 1997; Cox *et al*, 1998; Carmell *et al*, 2007; Houwing *et al*, 2007).

In the *Drosophila* ovary, two cytoplasmic PIWI paralogs, AGO3 and Aubergine (Aub), engage an amplification loop termed the “ping-pong cycle” to cleave both TE transcripts and long piRNA precursor transcripts arising from piRNA clusters, which comprise a large number as well as various types of fragmented TEs, leading to the post-transcriptional silencing of TEs and production of piRNAs (Brennecke *et al*, 2007; Gunawardane *et al*, 2007). These piRNAs can in turn trigger the production of phased piRNAs from piRNA precursors, which generates a dazzling variety of piRNAs and is coupled to the activity of a third Piwi protein (Han *et al*, 2015; Homolka *et al*, 2015; Mohn *et al*, 2015). Phased piRNAs are also produced in ovarian somatic cells by a ping-pong cycle-independent mechanism, which are in turn also loaded onto Piwi (Han *et al*, 2015; Mohn *et al*, 2015). This loading initiates the transport of Piwi into the nucleus where it drives the transcriptional silencing of target TEs, by inducing specific histone modification and/or facilitating the folding of chromatin into a higher-order structure (Iwasaki *et al*, 2016).

Lack of the nuclear Piwi activity results in de-repression of TEs, which is concomitant with decreases in both H3K9me3 repressive epigenetic marks and RNA polymerase II (Pol II) occupancy on target TE loci (Sienski *et al*, 2012; Donertas *et al*, 2013; Huang *et al*, 2013; Le Thomas *et al*, 2013; Ohtani *et al*, 2013; Rozhkov *et al*, 2013). This suggests a scenario of how the nuclear piRNA pathway

1 Department of Molecular Biology, Keio University School of Medicine, Tokyo, Japan

2 Graduate School of Engineering, Yokohama National University, Yokohama, Japan

3 Invertebrate Genetics Laboratory, National Institute of Genetics, Mishima, Shizuoka, Japan

4 Molecular Profiling Research Center for Drug Discovery, National Institute of Advanced Industrial Science and Technology, Tokyo, Japan

5 Department of Biological Sciences, Graduate School of Science, The University of Tokyo, Tokyo, Japan

\*Corresponding author. Tel: +81 3 5363 3529; E-mail: iwasaki@keio.jp

\*\*Corresponding author. Tel: +81 3 5363 3754; E-mail: awa403@keio.jp

†These authors contributed equally to this work

works: Piwi and its bound piRNAs scan for target TEs by complementary base-pairing with their nascent transcripts. Upon targeting, Piwi recruits chromatin factors including H3K9me3 methyltransferases such as Egless (also called dSetDB1) to initiate heterochromatin formation. The H3K9me3 modification is then bound by HP1a to maintain and propagate epigenetic silencing. However, thus far, direct association of the Piwi–piRNA complex with target transcripts and/or H3K9me3 methyltransferases has not been demonstrated.

Furthermore, depletion of Maelstrom (Mael), a Piwi cofactor in the nuclear piRNA pathway, does not decrease H3K9me3 levels at Piwi-targeted TE loci, suggesting that the repressive histone mark *per se* is not the final silencing mark for transcriptional gene silencing mediated by Piwi–piRNA complexes (Sienski *et al*, 2012). Recently, we identified linker histone H1 as a component of a nuclear Piwi complex and found that depletion of H1 de-represses Piwi-targeted TEs and their surrounding genes without affecting the density of H3K9me3 marks and HP1a at target TE loci (Iwasaki *et al*, 2016). Instead, we demonstrated that the chromatin accessibility at Piwi-targeted TE loci is modulated by H1. These findings suggested a model in which Piwi recruits H1 and forces it to stay on target TE loci to induce chromatin compaction, thereby repressing target TE transcription, and that the nuclear piRNA pathway adopts collaborated actions of H1 and H3K9me3 mark to maintain silencing of the TE state by modulating the chromatin state.

In addition to Mael and H1, biochemical and genetic analyses have also identified a number of putative Piwi cofactors including DmGTSF1/Asterix (Arx) and Panoramix (Panx)/Silencio (Brower-Toland *et al*, 2007; Wang & Elgin, 2011; Sienski *et al*, 2012, 2015; Czech *et al*, 2013; Donertas *et al*, 2013; Le Thomas *et al*, 2013; Muerdter *et al*, 2013; Ohtani *et al*, 2013; Yu *et al*, 2015). These findings together suggest that multiple pathways leading to Piwi-mediated TE silencing may exist, and raise the question of whether these pathways are independently initiated or have a common initial event.

To investigate this issue, we reanalyzed Panx, which interacts with Piwi and promotes the deposition of H3K9me3 marks on target TE chromatin by H3K9me3 histone methyltransferase, Egless (Sienski *et al*, 2015; Yu *et al*, 2015). Here, we biochemically isolated Nxf2, nuclear RNA export factor (NXF) variant, as a component of Panx-associated complexes. Nxf2 further associates with p15 (also called Nxt1), a co-adaptor for nuclear RNA export (Fribourg *et al*, 2001; Herold *et al*, 2001; Kerkow *et al*, 2012). The NXF family comprises four members in *Drosophila*, among which Nxf1 is an essential mRNA nucleocytoplasmic export factor (Izaurralde, 2002; Stutz & Izaurralde, 2003; Bjork & Wieslander, 2014; Wickramasinghe & Laskey, 2015). However, other members (Nxf2–4) are gonad-specific and their functions are not known, although they share common domain structures with Nxf1 (Herold *et al*, 2000, 2001, 2003). Detailed analysis of Nxf2 function in the nuclear piRNA pathway revealed that the interactions between Panx, Nxf2, and p15 are necessary to maintain the protein stability of Nxf2 and Panx. Moreover, ectopic targeting of Nxf2 initiates co-transcriptional repression of the target reporter gene prior to heterochromatin formation, and H3K9me3 marks and H1 are required at later time points. Notably, the RNA binding domain of Nxf2 is essential for recruitment of the complex to target TEs. CLIP experiments demonstrated that both Piwi and Nxf2 directly interact with Piwi-targeted TE transcripts and that the association of Nxf2 with target TE transcripts is Piwi-dependent. These results suggest that Nxf2 enforces

the association of Piwi–Panx–Nxf2–p15 (PPNP) complexes with the nascent transcripts of target TEs and triggers co-transcriptional repression in the nuclear silencing pathway.

## Results

### Nxf2 forms a complex with Piwi and Panx, and plays an essential role in the piRNA pathway

To reveal the precise mechanism by which Piwi–piRNA complexes transcriptionally silence TEs, we raised a monoclonal antibody that specifically recognizes Panx (Fig EV1A). Using this antibody, Panx-associated complexes were immunopurified from OSCs, a cultured ovarian somatic cell line, in which piRNA-guided silencing operates (Saito *et al*, 2009). Mass spectrometry analysis of the purified complexes (Fig 1A, Appendix Table S1) revealed that, in addition to Piwi, Nxf2 is present in the associated complexes. Nxf2 is a variant of the nuclear RNA export factor (NXF) family, which harbors similar domain structures (Herold *et al*, 2000, 2001, 2003; see also Fig EV1H). Among NXF variants, Nxf1 is highly conserved, ubiquitously expressed, and well known to be involved in the nuclear export of various mRNAs (Izaurralde, 2002; Stutz & Izaurralde, 2003; Bjork & Wieslander, 2014; Wickramasinghe & Laskey, 2015). However, Nxf2 and Nxf3 are almost exclusively expressed in the ovary, while Nxf4 is specifically expressed in the testis (Gramates *et al*, 2017). NXF variants other than Nxf1 are not involved in general mRNA export (Herold *et al*, 2001, 2003), and their functions remain to be revealed. By using a specific monoclonal antibody generated against Nxf2 (Fig EV1B), we confirmed the interaction among Panx, Piwi, and Nxf2 in both OSCs and *Drosophila* ovary (Fig EV1C and D). Immunoprecipitation followed by nuclear extraction also detected Piwi–Panx–Nxf2 complex (Figs 1B and EV1E and F). In addition, Panx and Nxf2 co-localized at the nucleus (Fig EV1G), suggesting that the complex is formed within the nucleus. The interaction of Panx with NXF variants is restricted to Nxf2 (Fig EV1H and I). Thus, we focused on the function of Nxf2 in the Piwi–piRNA pathway.

To identify transcripts regulated by Nxf2, we performed mRNA-seq analysis of OSCs under Nxf2 knockdown (KD) and compared the results with those obtained for Piwi- and Panx-KD OSCs (Figs 1C and D, and EV1J). TEs that were de-silenced upon Piwi depletion (Iwasaki *et al*, 2016) were also specifically de-silenced upon depletion of Panx or Nxf2. For example, *mdg1* and *gypsy* were among the most highly de-silenced TEs in Nxf2-, Panx-, and Piwi-KD experiments. Panx- and Nxf2-KD resulted in nearly identical patterns of TE de-silencing, albeit to a lesser extent than Piwi-KD, possibly because Piwi functions not only in TE silencing but also in piRNA biogenesis (see also Fig 1H). These results suggest that Nxf2 regulates TEs in the Piwi–piRNA pathway, in a manner resembling Panx, and are consistent with previous reports describing that Nxf2 was included in the list of candidate cofactors for the piRNA pathway identified by RNAi screening (Czech *et al*, 2013; Handler *et al*, 2013; Muerdter *et al*, 2013).

Depletion of Piwi has been shown to result in the reduction of H3K9me3 marks and H1 in the regions neighboring TE insertions, resulting in de-repression of coding genes located near TEs (Sienski *et al*, 2012; Iwasaki *et al*, 2016). Coding genes that were

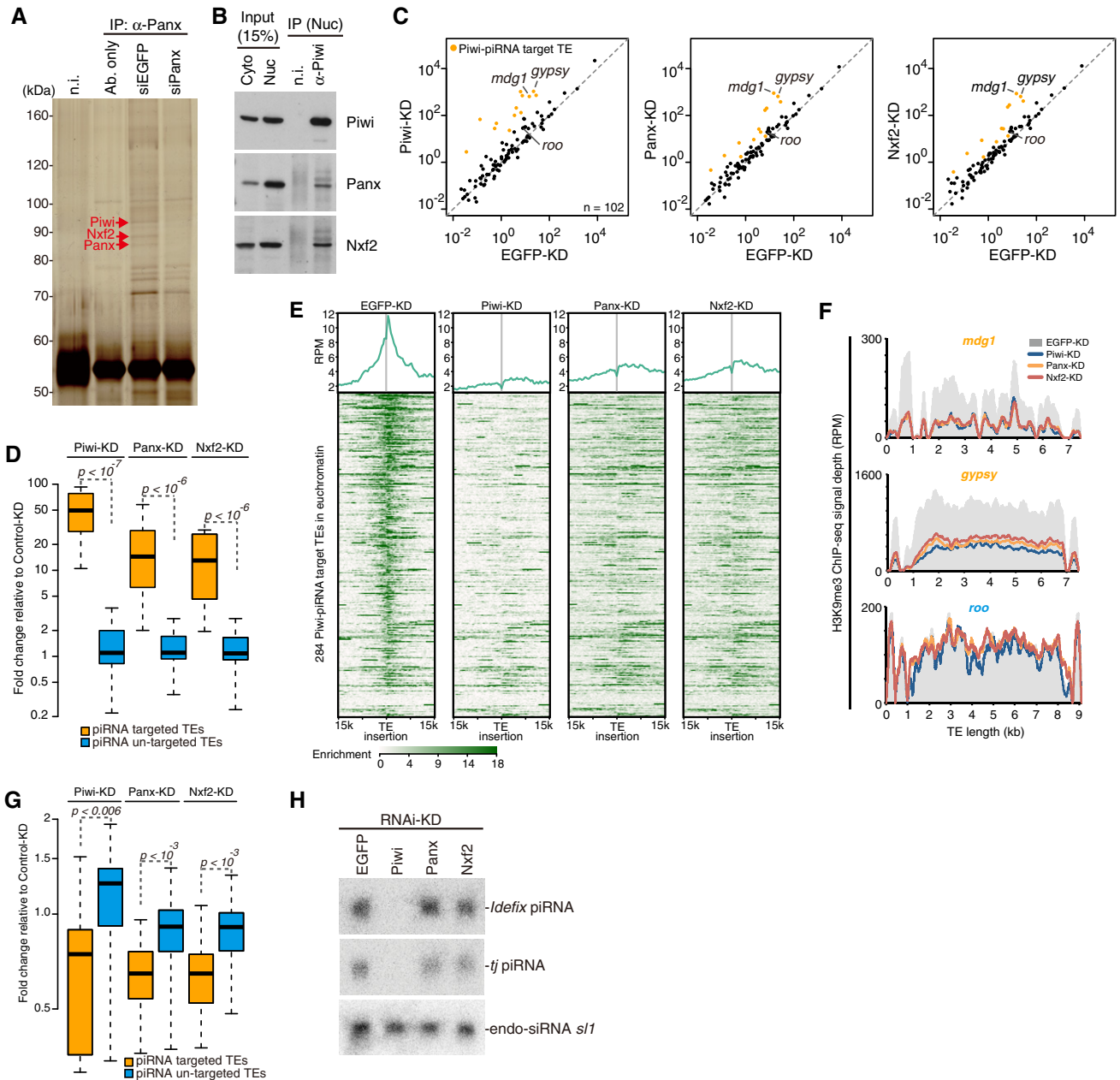


**Figure 1. Nxf2 is required for Piwi-piRNA-mediated TE silencing in OSCs.**

- A Immunoprecipitation (IP) from siRNA-transfected OSC lysate using anti-Panx antibody, followed by silver staining. Protein bands indicated by red arrows were identified by mass spectrometry analyses (see also Appendix Table S1). Mouse immunoglobulin G (IgG) (n.i.) was used for control IP.
- B IP from OSC lysate using anti-Piwi antibody, followed by Western blotting. Cyto: cytoplasmic fraction of OSCs. Nuc: nuclear fraction of OSCs.
- C Scatterplot of RPKM values for TEs in EGFP- (control), Panx-, or Nxf2-KD samples, based on RNA-seq. TEs for which the expression level differed from that of the control by more than tenfold in Piwi-KD (Piwi-piRNA-targeted TEs) are plotted in orange. Both x-axis and y-axis are a  $\log_{10}$  scale.
- D Boxplots showing fold changes in the expression of Piwi-piRNA-targeted and un-targeted TEs based on RNA-seq upon the indicated KD. Piwi-piRNA-targeted TEs are as defined previously (Iwasaki et al, 2016). Boxplot central bands, boxes, and whiskers show median, third quartile, first quartile, maxima, and minima, respectively.  $P$ -values were calculated by Wilcoxon rank-sum test, and the y-axis is a  $\log_2$  scale.
- E Meta-plot and heatmap indicating H3K9me3 levels within 15 kb of the Piwi-piRNA-targeted TE insertion are shown for OSCs with the indicated KD. Heatmap is sorted by the decrease of H3K9me3 levels in Piwi-KD against EGFP-KD.
- F Density plots for normalized H3K9me3 ChIP-seq signals over the consensus sequence from *mdg1*, *gypsy* (targeted by Piwi-piRNA, orange), and *roo* (not targeted by Piwi-piRNA, blue) TEs in EGFP-, Piwi-, Panx-, and Nxf2-KD OSCs.
- G Boxplots as in (D) showing fold changes in the H3K9me3 levels of Piwi-piRNA-targeted and un-targeted TEs upon the indicated KD.
- H Northern blotting for *Idefix*-piRNA, *traffic jam* (*tj*)-piRNA, and esiRNA *s1* (control) on total RNA isolated from OSCs with the indicated KD.

Source data are available online for this figure.

de-repressed upon Nxf2-KD were highly similar to those observed in Piwi-KD, suggesting that Nxf2 also regulates genes located near TE insertions. The population of differentially expressed genes (DEGs) and their fold change were smaller in Nxf2-KD (Fig EV1K–M), in line with the lower extent of TE de-silencing in Nxf2-KD (Fig 1C and D). These results indicate that Nxf2 functions in the Piwi–piRNA pathway and does not affect the expression pattern of bulk mRNA, consistent with the previous finding that Nxf1 is the only member of the *Drosophila* NXF family that mediates the export of mRNAs (Herold *et al*, 2001, 2003).

We further analyzed the H3K9me3 levels in these corresponding regions. ChIP-seq analysis of H3K9me3 marks at the euchromatic insertions of piRNA target TEs revealed that the depletion of Nxf2 decreased the H3K9me3 levels at these loci, similar to the case in Piwi or Panx depletion (Fig 1E–G). Notably, a severe decrease of H3K9me3 marks was observed not only at the TE insertions but also at the regions surrounding TE insertions (Fig 1E). The effect of Nxf2 or Panx depletion was weaker than that of Piwi depletion, and the results of Nxf2 and Panx depletion highly resembled each other, consistent with the effects on the expression levels of TEs observed by RNA-seq (Fig 1C and D). The analysis focusing on the TE consensus sequence confirmed that the effect on the H3K9me3 level was limited to the TEs targeted by Piwi–piRNA complexes (Fig 1G). Furthermore, the depletion of Nxf2 in OSCs did not affect the expression levels of piRNAs (Fig 1H), indicating that piRNA biogenesis including piRNA precursor export to the cytoplasm occurs in the absence of Nxf2. Together, these results indicate that Nxf2 is a key factor required for transcriptional silencing in the Piwi–piRNA pathway.

#### Formation of Panx–Nxf2–P15 complex is essential for stabilization of Panx and Nxf2 protein levels

To further characterize the Piwi–Panx–Nxf2 complex, we immunopurified flag-tagged Nxf2 expressed in OSCs (Fig EV2A), which was then subjected to shotgun proteome analysis (Fig EV2B, Appendix Table S2). This analysis not only confirmed the presence of Panx and Piwi, but further detected p15, also known as Nxt1, in Nxf2-associated complexes (see also Fig EV6C). p15 is a co-adaptor for nuclear RNA export and has been shown to form a heterodimeric complex with NXF proteins (Fribourg *et al*, 2001; Herold *et al*, 2001; Kerkow *et al*, 2012). We confirmed the interaction of Nxf2 with p15 in OSCs (Fig 2A), and p15 was also co-immunoprecipitated with Panx (Fig EV2C). These results suggest the formation of a Piwi–Panx–Nxf2–p15 complex, which we hereafter call the PPNP complex. Both Nxf1 and p15 are highly conserved from yeast to mammals, and the Nxf1–p15 complexes bind to mRNAs without strong sequence preference and have the ability to export mRNAs through the nuclear pore complex (NPC; Herold *et al*, 2001; Levesque *et al*, 2001; Wilkie *et al*, 2001; Wiegand *et al*, 2002). Although a previous study showed that recombinant p15 can associate with Nxf1, Nxf2, and Nxf3 proteins, only the Nxf1–p15 complexes function in mRNA export, and the role of p15's association with Nxf2 and Nxf3 remains unknown (Herold *et al*, 2001). We therefore analyzed the involvement of p15 in Nxf2-mediated transcriptional silencing.

Depletion of p15 resulted in specific de-repression of Piwi–piRNA-targeted TEs (Fig 2B). It was previously shown that p15 heterodimerizes with human and *C. elegans* Nxf1 at its NTF2

(nuclear transport factor 2)-like domains (Fribourg *et al*, 2001; Klenov *et al*, 2014). We therefore analyzed the interaction between p15 and Nxf2 mutant without NTF2-like domain (Fig EV2D and E). This mutant could not associate with p15, and the rescue experiment showed that the NTF2-like domain of Nxf2 is indispensable for the silencing of *mdg1* TE (Fig EV2F). These results suggest that the NTF2-like domain of Nxf2 associates with p15, as in the case of Nxf1, and this association is necessary for TE silencing.

Interestingly, depletion of p15 resulted in decreased levels of both Nxf2 and Panx proteins (Fig 2C). Since the RNA levels of Nxf2 and Panx remained unchanged in the p15-depleted samples (Fig 2D), p15 likely affects the stability of Nxf2 and Panx proteins. The protein level of p15 was unaffected by Nxf2-KD, possibly because p15 can bind to the other NXF proteins once Nxf2 is depleted (Fig 2C). De-silencing of the TEs and protein levels of Nxf2 and Panx could be rescued by expressing myc–p15 protein in p15-depleted OSCs (Fig 2E and F). Thus, p15 is an essential partner protein for Nxf2 to transcriptionally regulate Piwi–piRNA-targeted TEs, by stabilizing protein levels of Panx and Nxf2.

Notably, the knockdown of Nxf2 resulted in a severe decrease in the level of Panx protein (Fig 2C and G). A similar finding was observed in Panx-KD, where the level of Nxf2 protein was greatly decreased (Fig 2G). In contrast, neither Nxf2- nor Panx-KD affected the level of Piwi protein. RNA levels of Piwi, Panx, and Nxf2 in KD samples were determined by qRT–PCR, which showed that the levels of Panx and Nxf2 transcripts remained unchanged upon the knockdown of Nxf2 or Panx (Fig 2H). Destabilization of Panx upon Nxf2-KD was also observed in the germ cells of the ovary (Fig EV2G and H). Although the morphology of the ovary was not affected by the silencing of Nxf2 in the germline cells (Fig EV2H), severe fertility defects were observed: Flies with Nxf2 knockdown could lay eggs like the control flies, but none of them hatched (Fig EV2I). This phenotype was similar to that observed in flies expressing Piwi only in ovarian somatic cells but not germ cells (Jin *et al*, 2013). Additionally, TEs targeted by piRNAs in the germline were specifically de-silenced in Nxf2-depleted flies (Fig EV2J). These results together show that the Panx–Nxf2–P15 complex formation stabilizes the protein levels of Nxf2 and Panx (see also Figs 5 and EV5), and this is essential for TE silencing.

#### Tethering of Nxf2 to nascent mRNA leads to co-transcriptional silencing

We made use of reporter constructs to analyze the precise steps that the PPNP complex takes to mediate transcriptional silencing. First, we constructed reporter constructs whose transcripts are targeted by piRNAs derived from the *flam* locus, a prototype piRNA cluster (Brennecke *et al*, 2007; Post *et al*, 2014) (Fig EV3A). The *luc* reporter gene containing *flam* fragments in sense orientation or in antisense orientation relative to the *luc* transcripts was transfected into OSCs; it was shown that only the antisense reporters were strongly silenced (Fig EV3B–D). The antisense reporters were de-silenced in OSCs upon Piwi-KD (Fig EV3E) or depletion of Piwi cofactors, including Panx and Nxf2 (Fig EV3F), indicating that these factors were required for the co-transcriptional silencing in the Piwi–piRNA-targeted reporter system.

Previously, it was shown that the artificial recruitment of Panx can induce transcriptional silencing in *Drosophila* ovary (Sienski



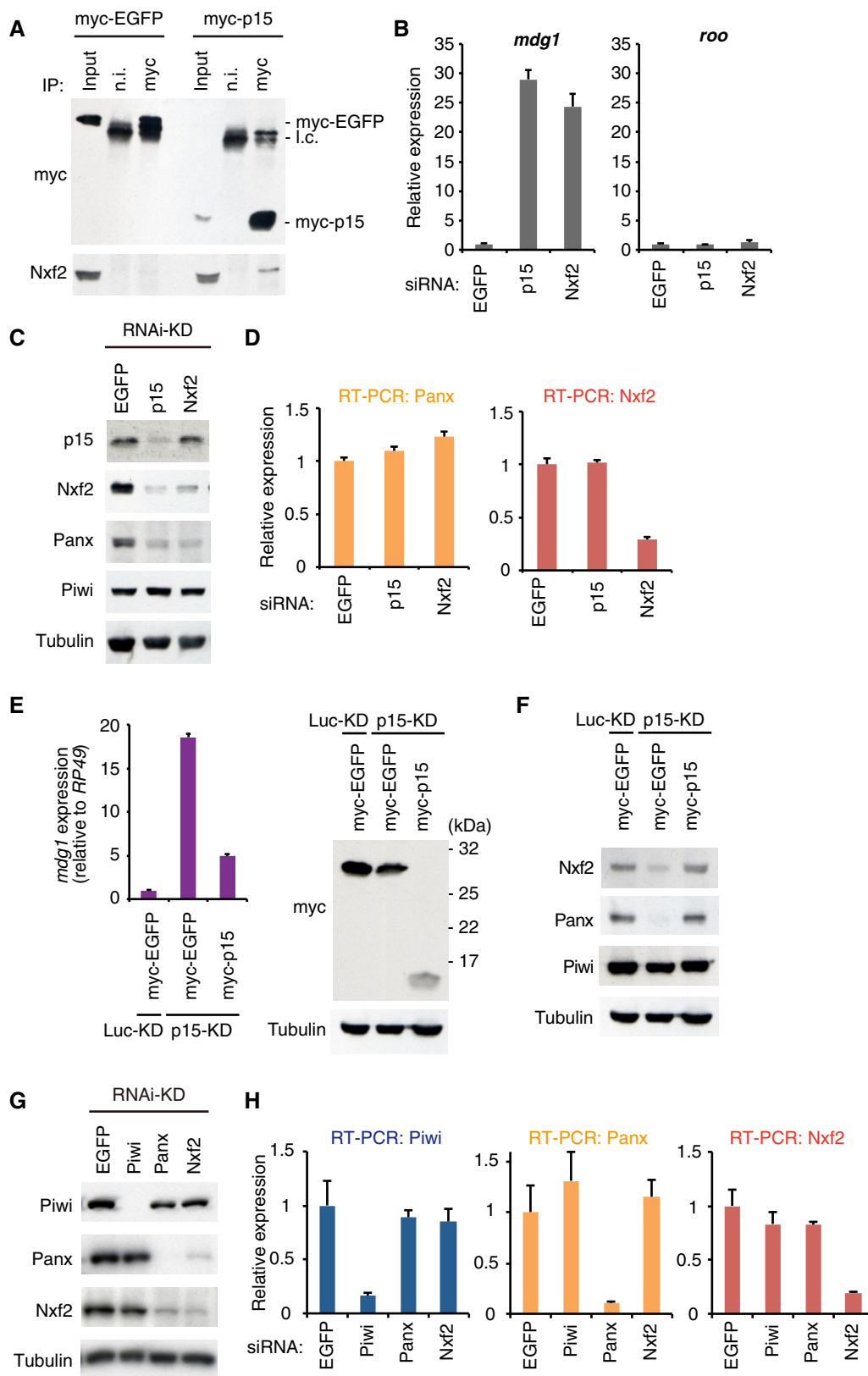


Figure 2.

**Figure 2. Panx–Nxf2–P15 complex formation is essential for the protein stability of Panx and Nxf2.**

- A Western blot (WB) showing Nxf2 protein levels in the complex immunoprecipitated from OSCs expressing either myc-EGFP or myc-p15, using myc antibody. Mouse immunoglobulin G (IgG) (n.i.) was used for control immunoprecipitation.
- B RNA levels of *mdg1* and *roo* were quantified by qRT–PCR upon depletion of EGFP (control), p15, or Nxf2. Error bars indicate SD ( $n = 3$ ). Note that KD was performed for 2 days with a single siRNA transfection for this experiment.
- C WB showing p15, Nxf2, Panx, Piwi, and Tubulin (loading control) protein levels upon EGFP (control)-, p15-, or Nxf2-KD.
- D RNA levels of Panx and Nxf2 were quantified by qRT–PCR upon depletion of EGFP (control), p15, or Nxf2. Error bars indicate SD ( $n = 3$ ).
- E myc-EGFP or myc-p15 was expressed in Luc- (control) or p15-depleted OSCs, and *mdg1* expression levels were monitored by qRT–PCR (left panel). Expression values are normalized by the expression of *RP49*. Error bars indicate SD ( $n = 3$ ). Using the same samples, WB was performed using antibodies against myc and Tubulin (right panel).
- F myc-EGFP or myc-p15 was expressed in Luc- (control) or p15-depleted OSCs, and WB was performed using antibodies against Nxf2, Panx, Piwi, and Tubulin.
- G WB showing Piwi, Panx, Nxf2, and Tubulin (loading control) protein levels upon EGFP (control)-, Piwi-, Panx-, or Nxf2-KD.
- H RNA levels of Piwi, Panx, and Nxf2 were quantified by qRT–PCR upon depletion of EGFP (control), Piwi, Panx, or Nxf2. Error bars represent SD ( $n = 3$ ).

Source data are available online for this figure.

*et al*, 2015; Yu *et al*, 2015). For further functional analysis of Nxf2 in the Piwi–piRNA silencing pathway, we took advantage of the  $\lambda$ N-boxB tethering system, in which  $\lambda$ N fusion proteins are delivered to a reporter RNA via protein–RNA interaction (Baron-Benhamou *et al*, 2004). We established a tethering system using OSCs carrying a genome-integrated luciferase (*luc*) reporter driven by the ubiquitin promoter, which harbors 14 boxB sites in its intron (Fig 3A). Expression of  $\lambda$ N-HA-tagged Nxf2 or Panx led to reporter silencing in a manner dependent on the  $\lambda$ N peptide fused to Nxf2 or Panx (Figs 3B and EV4A). Silencing induced by tethered Panx or Nxf2 results in strongly reduced *luc* RNA levels (Fig 3C). Knockdown of Panx and p15 weakened the repression by the enforced tethering of Nxf2, showing that Nxf2 needs Panx and p15 for efficient repression (Fig 3D). Consistent with previous reports (Sienski *et al*, 2015; Yu *et al*, 2015), the tethering of Piwi to the reporter failed to induce silencing (Fig 3B and C).  $\lambda$ N-HA-myc-tagged Piwi localized at the nucleus (Fig EV4B), indicating that  $\lambda$ N-HA-myc-tagged Piwi harbored piRNA in OSCs (Saito *et al*, 2010; Yashiro *et al*, 2018). Because Piwi, which is guided to the target reporter via loaded piRNA, represses its targets (Fig EV3), it is likely that only piRNA-guided Piwi is able to recruit silencing machinery to the target (see also Appendix Fig S2I).

To rule out the possibility that  $\lambda$ N-Nxf2 interferes with the splicing of the reporter mRNA, we constructed a *luc* reporter with 10 boxB sites in the 3' untranslated region (Fig EV4C). Tethering of Nxf2 to the reporter mRNA also led to silencing in a  $\lambda$ N peptide-dependent manner. To corroborate the results, we used an *in vivo* RNA-tethering system in the *Drosophila* ovary (Sienski *et al*, 2015). The expression of  $\lambda$ N-Nxf2 with the MTD-Gal4 driver (Fig EV4D) led to potent reporter silencing in germline cells but not in somatic cells of the ovary. Panx and Nxf2 proteins need to associate with each other to ensure their stability (Figs 2G and EV2G); therefore, it is likely that tethering of Panx results in the recruitment of Nxf2, and *vice versa*. These results indicate that the Nxf2–Panx complex is sufficient to induce co-transcriptional silencing, when targeted to nascent RNA.

To dissect the mechanism of the observed co-transcriptional gene silencing in the tethering system in OSCs, we depleted the expression of genes known to be associated with Panx (Fig EV1C) and involved in piRNA-directed transcriptional gene silencing. Depletion of Piwi or known Piwi cofactors (Gtsf1 (Sienski *et al*, 2012; Donertas *et al*, 2013; Ohtani *et al*, 2013) and Mael (Sienski *et al*, 2012)) instead had no impact on the Nxf2-mediated repression (Figs 3E and EV4E). Thus, Nxf2 acts with Panx most likely downstream from

Piwi and Gtsf1. Deficiency of Mael, however, does not result in decrease of H3K9me3 marks (Sienski *et al*, 2012), and thus, Mael may act in parallel to the silencing mediated by the Piwi–Panx–Nxf2 complex; knockdown of each component of the complex all results in depletion of H3K9me3 marks.

Furthermore, we examined the roles of chromatin-related factors in co-transcriptional silencing mediated by Piwi–piRNA complexes. Depletion of Eggless had no effect on the silencing by  $\lambda$ N-Nxf2 in the tethering system using OSCs (Figs 3F and EV4F). In addition to Eggless-KD, H1-KD and HP1-KD also had no impact on the silencing by Piwi–piRNA and  $\lambda$ N-Nxf2 in the reporter system based on plasmids (Figs EV3F and EV4G–J). While this result is consistent with a report of a study using a plasmid-based reporter assay to detect Piwi-directed silencing in *Drosophila* ovary somatic sheet cells (Clark *et al*, 2017), it is at odds with previous reports demonstrating that the methyltransferase Eggless is required for Panx-mediated silencing using the tethering system in the *Drosophila* ovary (Sienski *et al*, 2015; Yu *et al*, 2015). These conflicting results are probably due to the different expression systems of  $\lambda$ N fusion proteins.  $\lambda$ N fusion proteins are driven by MTD-Gal4 constitutively in the tethering system in the ovary, whereas they are expressed transiently by DNA transfection in the tethering system using OSCs. The tethering system in the ovary probably enables us to observe late phases of a suppressed state of the reporter gene. In contrast, transient expression of  $\lambda$ N fusion proteins makes it possible to analyze the mechanism of transition from initiation to the fully suppressed state of the reporter gene in our tethering system using OSCs. The results of Eggless-KD upon tethering of  $\lambda$ N-Nxf2 suggest that the Nxf2–Panx pair elicits co-transcriptional repression prior to heterochromatin formation on TEs in the Piwi–piRNA pathway.

### Nxf2 triggers co-transcriptional repression prior to heterochromatin formation

To elucidate the precise mechanism by which  $\lambda$ N-Nxf2 represses the reporter gene integrated in the genome, we examined the time course of silencing by  $\lambda$ N-Nxf2, which was expressed in OSCs by transient transfection of expression vector. The expression level of  $\lambda$ N-Nxf2 gradually decreased with a peak at 36 h post-transfection (hpt), and it had dropped below the detection limit at 96 hpt (Fig 4A). The luciferase activity reached its bottom at 48 hpt and remained suppressed at 96 hpt despite the absence of  $\lambda$ N-Nxf2. Consistent with these observations, the level of Pol II association with the reporter gene decreased at 48 and 96 hpt (Fig 4B). Notably,

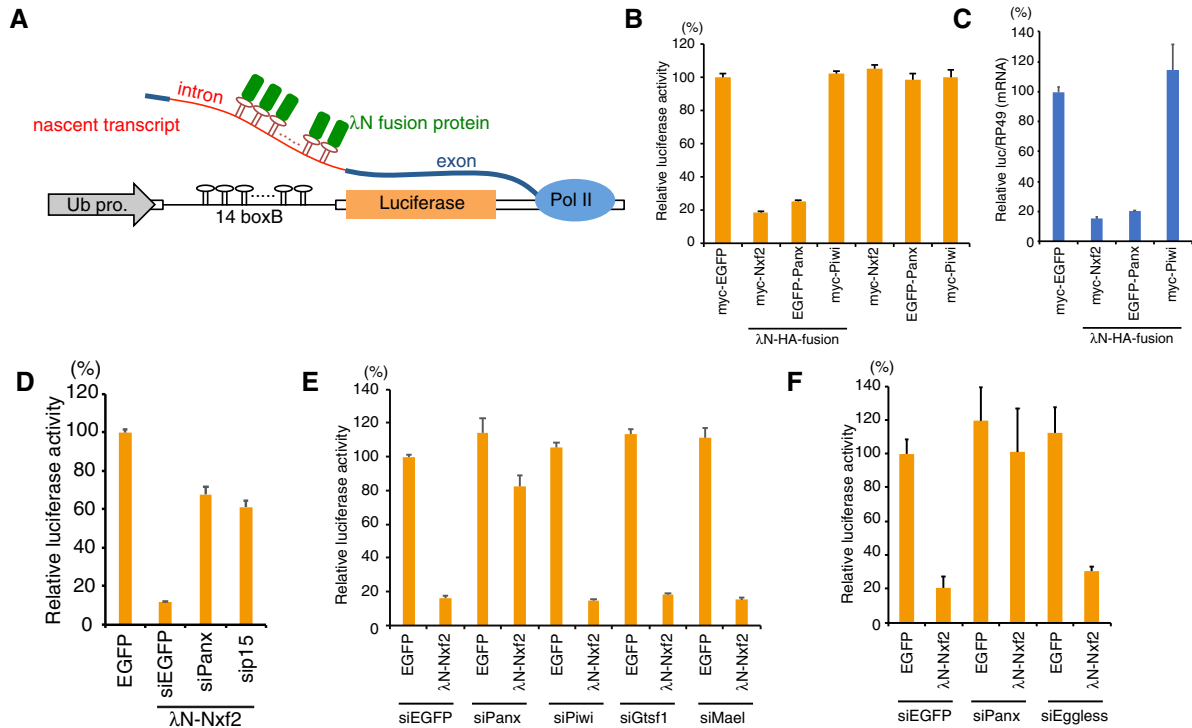


**Figure 3. Nxf2 tethered to nascent mRNA causes co-transcriptional silencing.**

- A** Schematic of boxB-λN tethering system in OSCs. A genome-integrated luciferase reporter with 14 copies of boxB sites located within the intronic region of ubiquitin (Ub). λN fusion proteins are recruited to luciferase reporter RNA via 14× boxB.
- B** Effects on luciferase activity of the proteins indicated below. OSCs carrying the reporter gene were transfected with plasmids expressing the indicated proteins and were harvested at 48 h post-transfection (hpt). Luciferase activities were normalized by the total protein amount. Bar graph shows luciferase activity relative to that of myc-EGFP (control). Error bars indicate SD ( $n = 4$ ).
- C** qRT-PCR showing effects of the indicated λN fusion proteins on *Luc* mRNA level at 48 hpt. Levels of *Luc* mRNA were normalized by *RP49* mRNA. Bar graph shows the level of *Luc* mRNA relative to myc-EGFP (control). Error bars indicate SD ( $n = 6$ ).
- D** Silencing by the enforced tethering of Nxf2 shows Panx- and p15-dependent manner. Bar graph shows luciferase activity relative to that of the sample transfected with EGFP expression vector (control). Error bars indicate SD ( $n = 3$ ).
- E, F** Effects of knockdown of the indicated genes on luciferase activity upon λN-Nxf2 expression at 48 hpt. Bar graph shows luciferase activity relative to that of the sample co-transfected with myc-EGFP and siEGFP (control). Error bars indicate SD ( $n = 3$ ).

no significant difference was observed in the occupancies of H1 and H3K9me3 at 48 hpt, despite λN-Nxf2 repressed the reporter gene (Fig 4A and C). This can be interpreted to mean that Nxf2-triggered co-transcriptional repression is independent of chromatin factors. By contrast, H1 and H3K9me3 accumulated on the reporter gene at 96 hpt (Fig 4C), suggesting that heterochromatin is formed at this time point on the reporter gene in the absence of λN-Nxf2, leading to continued silencing. To verify the role of heterochromatin formation in the gene silencing induced by λN-Nxf2, we knocked down H1 or HP1a after expression of λN-Nxf2. The effects of H1- and HP1a-KD on the λN-Nxf2-mediated silencing were negligible at 48 hpt (Fig 4D). To examine the roles of H1 and HP1a in the λN-Nxf2-mediated silencing at the latter time point, we determined luciferase activity at 96 hpt of the λN-Nxf2 expression vector followed by H1- and HP1a-KD. The depletion of H1 or HP1a partially restored luciferase activities upon tethering of λN-Nxf2 at 96 hpt (Fig 4E). These findings together suggest that λN-Nxf2 may initiate co-transcriptional repression prior to heterochromatin formation mediated by H1 and HP1a, which is required for maintaining the suppressed state of the reporter gene in the latter stage of silencing when little

or no λN-Nxf2 is present. In other words, the silencing mode mediated by tethered Nxf2 may switch from Nxf2–Panx-dependent to heterochromatin-dependent.

### The first LRR region of Nxf2 harbors RNA binding activity and is necessary for piRNA-mediated transcriptional silencing

To reveal the role of Nxf2 in the PPNP complex-mediated co-transcriptional silencing, we characterized the regions of Panx and Nxf2 proteins necessary for their function. This revealed that the middle region (300–399 aa) of Panx is necessary for its interaction with Nxf2 (Fig 5A and B), whereas its N-terminal region (1–169 aa) interacts with Piwi (Fig 5A and B). Rescue experiments and ectopic tethering experiments with the deletion mutants confirmed that both regions of Panx are indispensable for the transcriptional regulation (Fig EV5A and B). We also produced a series of Nxf2 deletion mutants (Fig 5C) and found that the C-terminal UBA (ubiquitin-associated) domain of Nxf2 is necessary for interaction with Panx (Fig 5D). Although Nxf1 also harbors a UBA domain, we did not detect interaction between Nxf1 and Panx, indicating that Panx

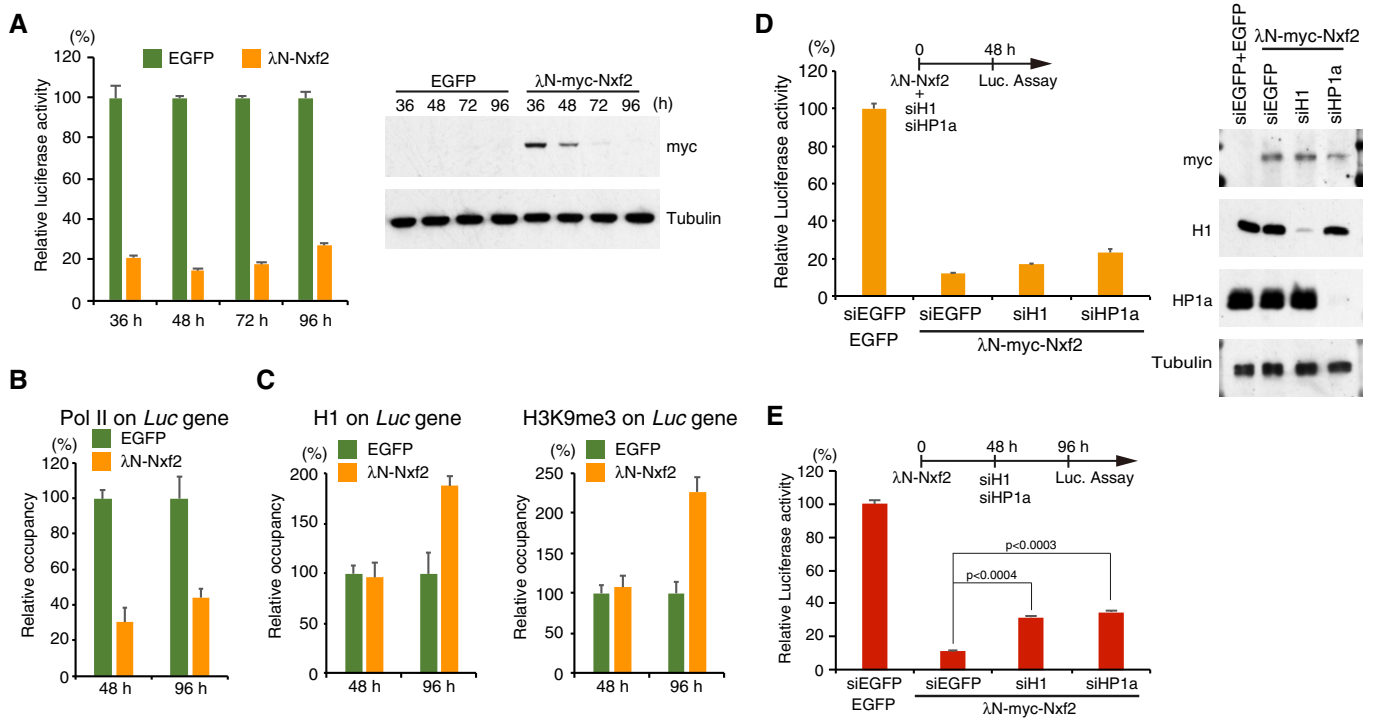


**Figure 4. Nxf2 initiates co-transcriptional silencing before heterochromatin formation.**

- A Time course of luciferase activity upon  $\lambda$ N-Nxf2 tethering. Bar graph shows luciferase activity relative to that of EGFP at the indicated incubation time. Error bars indicate SD ( $n = 3$ ) (left panel). Expression levels of myc-tagged  $\lambda$ N-Nxf2 were monitored using anti-myc antibody. Tubulin was used as a loading control (right panel).
- B ChIP-qPCR analysis of RNA polymerase II occupancy on the *Luc* gene upon  $\lambda$ N-Nxf2 tethering. Bar graph shows the occupancy relative to that of the sample transfected with a plasmid expressing EGFP. Error bars indicate SD ( $n = 3$ ).
- C ChIP-qPCR analysis of histone H1 and H3K9me3 occupancy on the *Luc* gene. Bar graph shows the occupancy relative to that of the sample transfected with a plasmid expressing EGFP. Error bars indicate SD ( $n = 3$ ).
- D Effects of H1 and HP1a on luciferase activity upon  $\lambda$ N-Nxf2 tethering at 48 hpt. OSCs were co-transfected with protein expression vectors and the indicated siRNAs and cultured for 48 h in accordance with the experimental scheme at the top of the figure. Bar graph shows luciferase activity relative to that of the sample expressing EGFP (control). Error bars indicate SD ( $n = 3$ ) (left panel). Western blots showing the protein levels of  $\lambda$ N-myc-Nxf2, H1, HP1a, and Tubulin (loading control) in the same samples (right panel).
- E Effects of H1 and HP1a on luciferase activity upon  $\lambda$ N-Nxf2 at 96 hpt. Transfection schedule of plasmids and siRNAs is shown at the top of the figure. siRNA transfection was carried out at 48 h, since the depletion effect reaches maximum after 48 hpt. Bar graph shows luciferase activity relative to that of the sample expressing EGFP (control). Error bars indicate SD ( $n = 3$ ). *P*-values were calculated by the Student's *t*-test.

specifically recognizes the UBA domain of Nxf2 (Fig EV11). These results suggest that the UBA domain of Nxf2 and middle region of Panx interact with each other, and N-terminal region of Panx is linked to Piwi.

Using the deletion mutants of Nxf2 (Fig 5C), we further performed rescue experiments by expressing each deletion mutant in Nxf2-depleted OSCs (Fig 5E). The expression of Panx protein could be stabilized not only by full-length Nxf2 but also by Nxf2- $\Delta$ LRR (leucine-rich repeat), showing that mutants that interact with Panx can rescue its protein level. However, Nxf2- $\Delta$ LRR, which associates with Panx and also Piwi (Figs 5D and EV5C), could not recover the silencing of *mdg1* TE, suggesting that the LRR region of Nxf2 has an essential function other than formation of the PPNP complex. Consistent with this, piRNA-targeted reporters that were de-silenced upon depletion of Nxf2 (Fig EV3F) could be rescued by full-length Nxf2, but not by Nxf2- $\Delta$ LRR (Fig EV5D). We next investigated which of the Nxf2 mutants could induce silencing, when tethered to the reporter gene (Fig 5F). Interestingly, in addition to full-length Nxf2,

Nxf2- $\Delta$ LRR mutant could induce silencing, indicating that the LRR region is dispensable once Nxf2 is tethered to the target gene. These results suggest that the LRR domain of Nxf2 is required to maintain recruitment of the PPNP complex to its targets.

It has been shown that Nxf1, the other NXF member in *Drosophila*, associates with bulk mRNA at its N-terminal RNA binding domain to induce its export (Viphakone *et al.*, 2012). Additionally, a human homolog of Nxf2 associates with RNA through its N-terminal region (1–377 aa; Herold *et al.*, 2000). Meanwhile, both Nxf1 and Nxf2 in human use the N-terminal region to bind Alyref, a key factor for recruitment of Nxf1 to mRNA (Herold *et al.*, 2000). To investigate the possible function of N-terminal region of *Drosophila* Nxf2 in piRNA pathway, we first performed knockdown of Alyref homolog in *Drosophila*. There are two homologs of Alyref in *Drosophila*, and Ref2 is not expressed in ovary nor OSCs (Gramates *et al.*, 2017). We therefore performed knockdown of Ref1, which did not result in de-silencing of *mdg1* TE (Fig EV5E). We further performed an electrophoretic mobility shift assay (EMSA) to analyze the RNA binding



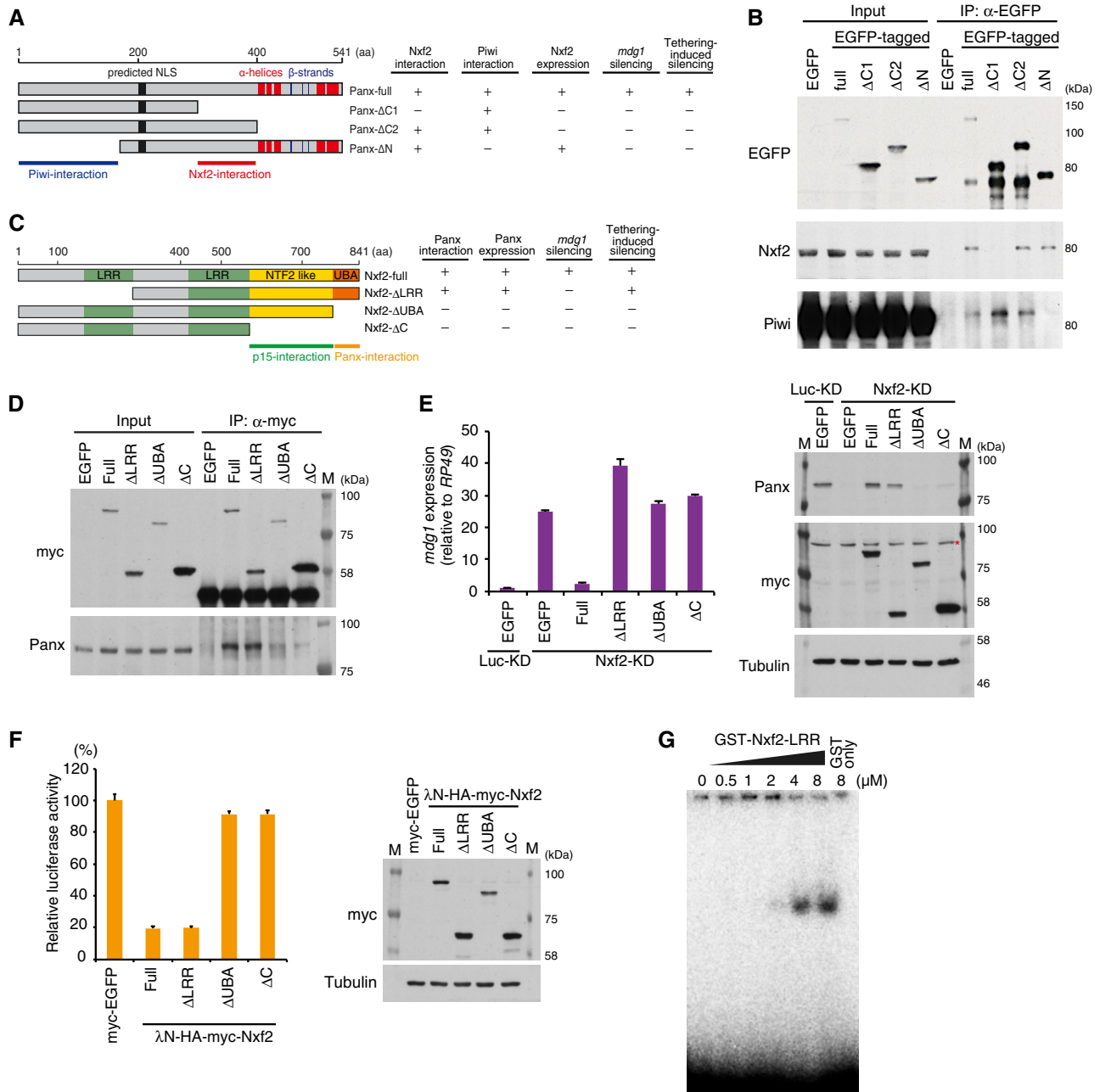


**Figure 5. Nxf2 associates with Piwi-piRNA silencing complex to target RNA via its first LRR region.**

- A Schematic of full-length Panx protein and deletion mutants. Predicted NLS and  $\alpha$ -helices and  $\beta$ -strands are indicated (left panel). The results of rescue experiments are summarized (right panel).
- B Western blot (WB) of EGFP-Immunoprecipitation (IP) product from lysate of EGFP-tagged Panx deletion construct-expressing OSCs, using EGFP, Nxf2, and Piwi antibody.
- C Schematic of full-length Nxf2 and deletion mutant proteins. LRR: leucine-rich repeat domain, NTF2-like: nuclear transport factor 2-like domain, UBA: ubiquitin-associated domain (left panel). The results of rescue experiments and tethering assay are summarized (right panel).
- D IP using anti-myc antibody from lysate of OSCs expressing myc-tagged Nxf2 proteins, followed by WB using anti-myc or anti-Panx antibody.
- E *mdg1* expression levels were monitored by qRT-PCR in OSCs expressing exogenous Nxf2 proteins treated with either siLuc (control) or siNxf2 (left panel). Error bars indicate SD ( $n = 3$ ). Exogenous Nxf2 mRNAs are resistant to siRNA for Nxf2. Expression levels of Panx- and myc-tagged Nxf2 proteins were confirmed by WB using anti-myc and anti-Panx antibodies. Tubulin was used as a loading control. Asterisk indicates the background signal (right panel).
- F Effects of  $\lambda$ N fusion Nxf2 proteins on luciferase activity at 48 hpt. Error bars indicate SD ( $n = 3$ ) (left panel). Expression levels of exogenous  $\lambda$ N-HA-myc-Nxf2 proteins (right panel).
- G Electrophoretic mobility shift assay (EMSA) showing the binding of the first LRR region of Nxf2 (1–285 aa) to single-stranded RNA. The indicated amount of recombinant protein was mixed with 1 nM single-stranded RNA (16 nt).

activity of the N-terminal LRR domain of Nxf2 and observed an association of single-stranded RNA with the purified GST-tagged first LRR domain of Nxf2 (1–285 aa) (Fig 5G). These results suggest that Nxf2 requires the LRR domain, which harbors RNA binding activity, in addition to the other domains necessary for formation of the PPNP complex, to tether the silencing complex to its target transcripts.

### Nxf2 directly interacts with piRNA-targeted TE transcripts in a Piwi-dependent manner

The RNA binding activity of Nxf2 prompted us to elucidate the mechanistic details of how Nxf2 is recruited to TE transcripts. We investigated cellular transcripts associated with Nxf2 and/or Piwi via UV cross-linking and immunoprecipitation (CLIP) assay (Flynn *et al*, 2015, Van Nostrand *et al*, 2016). We first raised a stable cell line of OSCs that express siRNA-resistant myc-Nxf2, since our Nxf2 antibody is not suitable for immunoprecipitation. The expression level of myc-Nxf2 is slightly higher than that of endogenous Nxf2, and Nxf2-siRNA specifically depletes endogenous Nxf2 (Fig EV6A). myc-Nxf2 forms a complex identified using antibody against endogenous Panx and is capable of silencing *mdg1* TEs (Fig EV6B and C). We therefore used this stable line to analyze the RNA population targeted by Nxf2.

We generated CLIP libraries using RNA isolated from myc-Nxf2 or Piwi immunoprecipitants. Immunoprecipitants were run on standard protein gels and transferred to nitrocellulose membranes, and a region 50 kDa above the protein size was excised for RNA isolation (Fig EV6D), referring to the eCLIP method (Van Nostrand *et al*, 2016). The same region was excised for the input sample in order to generate a size-matched input (SMInput) library, which enables efficient background normalization and then leads to a more accurate measure of the enrichment of CLIP signals (Van Nostrand *et al*, 2016). Each CLIP experiment was performed in two biological replicates, and the reads were merged after checking the correlation of read counts of annotated peaks (Fig EV6E). We first performed CLIP assay of myc-Nxf2 protein in UV-crosslinked and non-UV-crosslinked samples, to examine whether RNA associated with myc-Nxf2 could be captured by this assay. We observed a significant decrease in the amount of CLIP tags obtained for piRNA-targeted TE transcripts when CLIP was performed on non-UV-crosslinked samples (Fig EV6F), indicating that we can specifically capture target RNA by the myc-Nxf2 CLIP assay.

Based on these results, we further performed myc-Nxf2 CLIP assay upon control (EGFP) or Piwi knockdown. Endogenous Nxf2 was also depleted, in order to increase the ratio of functioning myc-Nxf2. We first compared the enrichment of obtained CLIP tags to that of SMInput control, for the reads mapped in the sense or antisense direction of TEs (Fig 6A). This revealed that there was some fraction of TEs with enrichment of CLIP tags mapped in the sense direction, whereas this enrichment was not observed for the reads mapped in the antisense direction. Additionally, we plotted the TEs targeted by Piwi-piRNA complexes, which showed that TEs with enriched CLIP tags were the targets of piRNAs (Fig 6A). Notably, the specific enrichment of myc-Nxf2 CLIP tags on piRNA-targeted TEs was lost upon the knockdown of Piwi (Figs 6B and EV6G, see also Fig 6D), indicating that Piwi is required for Nxf2 to specifically associate with piRNA-targeted transcripts.

To further investigate the relationship between RNA targeting of Nxf2 and Piwi, we performed Piwi CLIP assay. As in the case of

myc-Nxf2 CLIP, we observed the specific enrichment of CLIP tags against SMInput, specifically for those mapped in the sense direction of piRNA-targeted TEs (Fig 6C and D). We compared the expression level of TEs under Piwi-, Panx-, and Nxf2-KD, and also piRNA reads from Piwi-immunoprecipitant (Fig 6E). This revealed that TEs with enriched myc-Nxf2 and Piwi CLIP tags were depleted upon the depletion of Piwi, Panx, or Nxf2, and they were also targeted by piRNAs. A density plot of myc-Nxf2 and Piwi CLIP tags, along with piRNA reads, showed that myc-Nxf2 and Piwi CLIP tags had similar distributions, while piRNAs that can target wider regions of TEs were produced (Fig 6F). This indicates the possibility that specific piRNAs can silence certain transposons more efficiently than others. Since CLIP peaks tend to be detected on LTR regions or 5' regions of transposons, piRNAs may silence their targets as soon as they are transcribed, and therefore, downstream RNAs may not be produced. These results, together with the finding that PPNP association is essential in order to stabilize the protein level of Nxf2 (Fig 2), suggest that the PPNP complex is recruited to nascent transcripts by base-pairing of Piwi-associated piRNAs with targets, and further enforced through the RNA binding activity of Nxf2.

## Discussion

Here, we propose a model in which the engagement of the PPNP complex with nascent TE transcripts initiates co-transcriptional silencing prior to heterochromatin formation (Fig EV6H). Although the heterochromatin factors are not required for the initial step of the silencing (Fig 4), they play a significant role in maintenance of the repressed status in the later stages of TE silencing. Because the depletion of Piwi activity rapidly results in the de-repression of TEs (Fig 1), this also suggests that silencing initiation and heterochromatin formation undergo continuous cycling to enforce a silenced state of TEs.

Four groups including ours have obtained the similar findings regarding the essential role of Nxf2 in the Piwi-piRNA pathway rather than in nuclear RNA export (preprint: Batki *et al*, 2019; Fabry *et al*, 2019, preprint: Zhao *et al*, 2019). We all have identified a new complex of Panx-Nxf2-P15, which associates with Piwi. Although Batki *et al* and Fabry *et al* did not observe significant amount of Piwi peptides in their shotgun MS analysis of Panx immunoprecipitants, they showed the interaction between Panx-Piwi in immunoprecipitation followed by Western blot analysis and their former studies (preprint: Batki *et al*, 2019; Fabry *et al*, 2019; Sienski *et al*, 2015; Yu *et al*, 2015). The inconsistency could be due to the immunoprecipitation conditions and/or antibodies used. Additionally, we all have shown that the UBA domain of Nxf2 associates with Panx, and the NTF2 domain associates with p15. Our group and Batki *et al* have shown that the first LRR domain with RNA binding activity is needed for the regulation of TEs (preprint: Batki *et al*, 2019), and we have further shown direct association of TE transcripts with Nxf2 (Fig 6). Among these four groups, we were the only one which was able to observe the initial steps of the silencing. This is because we performed our analysis using cultured cell line OSCs, and took different timepoints after expression of Nxf2 (Fig 4). The present study is the only one to consider time points as early as 48 h. The regulation observed at

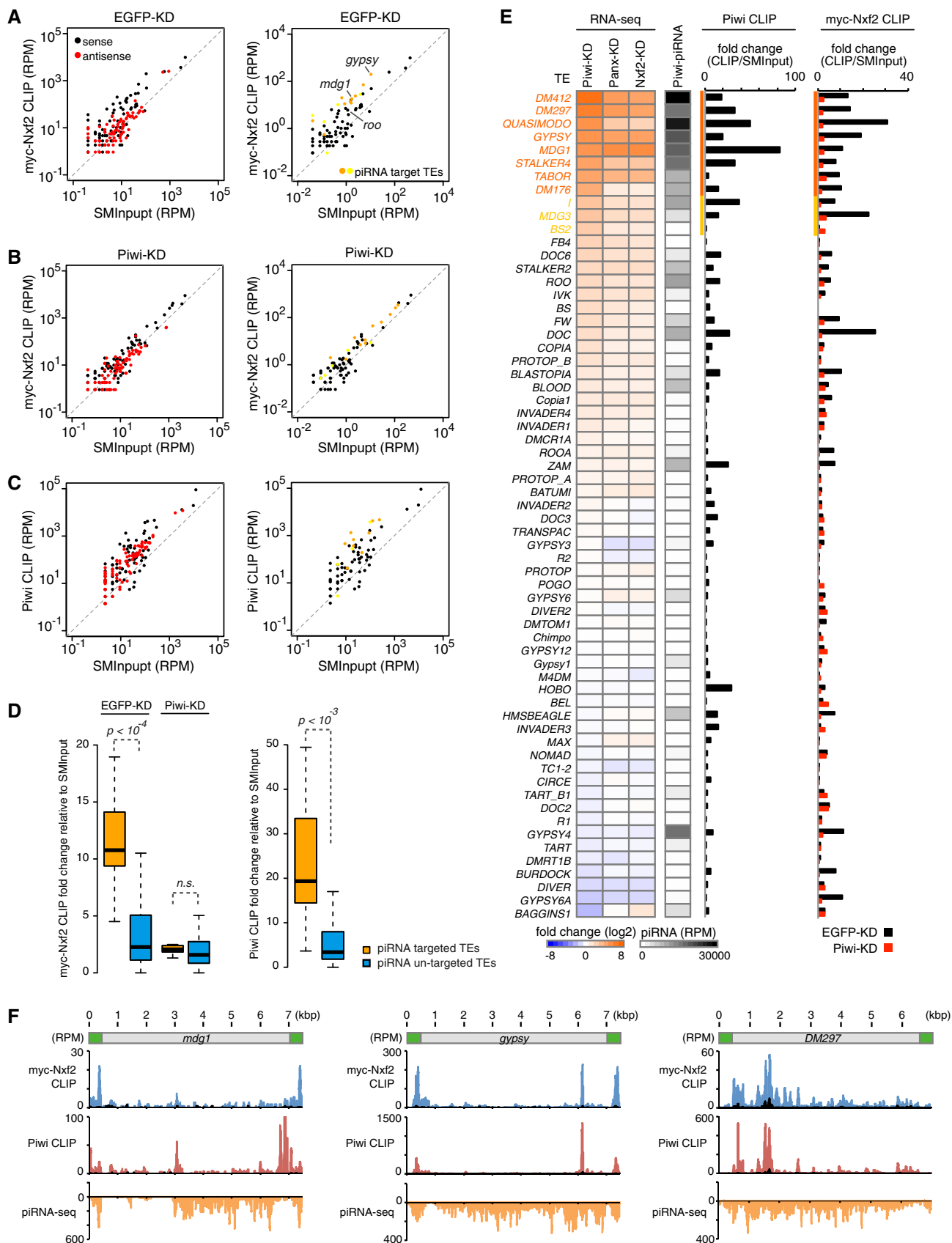


Figure 6.

**Figure 6. Nxf2 associates with nascent transcript of Piwi-piRNA-targeted TEs.**

- A Scatterplot of RPM values for myc-Nxf2 CLIP tags (y-axis) and SMIInput reads (x-axis) mapped to TEs in EGFP (control)-KD samples. Both x-axis and y-axis are  $\log_{10}$  scales. Sense reads are plotted in black and antisense reads in red (left panel). TEs for which the expression level differed from that of the control by more than tenfold or fivefold in Piwi-KD (Piwi-piRNA-targeted TEs) are plotted in orange or yellow, respectively (right panel).
- B Scatterplot as in (A). The plot was created using myc-Nxf2 CLIP data from Piwi-KD samples.
- C Scatterplot as in (A). The plot was created using Piwi CLIP data. Note that RNAs used for creating Piwi CLIP libraries are in the size range of 43–73 nt, and therefore, piRNAs are excluded.
- D Boxplots showing fold changes of the indicated CLIP tags to SMIInput, for Piwi-piRNA-targeted and un-targeted TEs. Piwi-piRNA-targeted TEs are defined based on RNA-seq analysis (Fig 1). Reads mapped to sense direction of indicated TEs were used for calculation of CLIP tag fold change, and TEs with SMIInput signal under 0.5 RPM were eliminated. Boxplot central bands, boxes, and whiskers show median, third quartile, first quartile, maxima, and minima, respectively. *P*-values were calculated by the Wilcoxon rank-sum test. n.s., not significant, *P* > 0.01.
- E Heatmaps displaying fold changes of TE expression with indicated siRNA knockdown (normalized to EGFP-KD), and Piwi-associated piRNA levels obtained from small RNA-seq (RPM). The CLIP-seq diagram indicates fold changes of Piwi CLIP tags, and myc-Nxf2 CLIP tags relative to SMIInput, obtained upon EGFP- or Piwi-KD. Reads mapped to sense direction of indicated TEs were used for calculation of CLIP tag fold change, and TEs with SMIInput signal under 0.5 RPM were eliminated. Piwi-bound piRNA levels were determined by using reads mapped to antisense of the indicated TEs. TEs for which the expression level differed from that of the control by more than tenfold or fivefold in Piwi-KD (Piwi-piRNA-targeted TEs) are indicated in orange or yellow, respectively.
- F Density plots for myc-Nxf2 CLIP tags (blue plots), Piwi CLIP tags (red plots), and Piwi-piRNA reads (orange plots) over the consensus sequence from *mdg1*, *gypsy*, and *DM297* (Piwi-piRNA target TEs). The LTR region of each TE is illustrated in green. SMIInput is overlaid in black at each plot; y-axis has been adjusted to 100 for the plot of Piwi CLIP tags mapped to *mdg1*.

96 h after transfection, representing later stages of TE silencing, was consistent with the observation by Batki *et al* (preprint: Batki *et al*, 2019). An important issue to be clarified is the mechanism by which the PPNP complex initiates the silencing of TEs.

In *C. elegans*, NRDE-2 (nuclear RNAi defective-2) associates with the Argonaute protein NRDE-3 in the nucleus and is recruited by the NRDE-3/siRNA complex to nascent transcripts. This complex inhibits Pol II during the elongation and directs the accumulation of Pol II at genomic loci targeted by RNAi (Guang *et al*, 2010). We investigated whether  $\lambda$ N-Nxf2 directs the accumulation of Pol II at boxB sites in the co-transcriptional silencing (Appendix Fig S1A–C). Although the time course of Pol II occupancy upon  $\lambda$ N-Nxf2 was examined by ChIP-qPCR at the boxB sites, we could not observe any accumulation of Pol II along the reporter gene.

Recently, it was reported that Pol II-associated proteins, PAF1 and RTF1, antagonize Piwi-directed silencing (Clark *et al*, 2017), which are factors involved in the modulation of promoter release, elongation, and termination of Pol II (Chen *et al*, 2015; Van Oss *et al*, 2017; Vos *et al*, 2018). The Panx-Nxf2-P15 complex might interfere with Pol II via the PAF1 complex, considering that fission yeast PAF1 represses AGO1/siRNA-directed silencing (Kowalik *et al*, 2015). Although we examined the effect of PAF1 and RTF1 on the co-transcriptional silencing, PAF1 and RTF1 do not appear to be involved in the co-transcriptional silencing mediated by  $\lambda$ N-Nxf2 (Appendix Fig S1D–I). These results suggest that Pol II regulation by the PPNP complex differs from that of the small RNA-mediated Pol II regulation model proposed previously. It may be necessary to identify key factors involved in this regulation, possibly by performing proteome analysis of the unknown factors tethered to our reporter recruitment system.

We found a decrease in the active histone H3K4me3 marks on the reporter gene even at an earlier time point (48 hpt) at which the level of H3K9me3 marks remained low (Appendix Fig S2A and B, Fig 4C). Two reports about H3K4 methylation in Piwi-mediated silencing have been published. The level of H3K4 methylation on TEs is increased upon Piwi-KD (Klenov *et al*, 2014). The expression of artificial piRNAs that target a reporter locus induced transcriptional silencing associated with a decrease in the active H3K4-methylation marks (Le Thomas *et al*, 2013). In addition, the depletion of LSD1, which removes H3K4-methylation marks from promoters, had significant effects on the ability of Panx to repress the reporter gene (Yu *et al*, 2015). Therefore, we

performed LSD1-KD and examined the effect of LSD1 on co-transcriptional silencing by the enforced tethering of Nxf2. However, the depletion of LSD1 had a limited impact on the silencing, whereas the level of *mdg1* was increased 27-fold upon LSD1-KD (Appendix Fig S2C–G). These findings together suggest that the decrease observed in H3K4me3 levels at 48 hpt in the tethering assay may not have been due to LSD1.

Nxf2 is the core factor of the PPNP complex, and our results suggest that the nuclear export factor variant has been co-opted to repress TEs in the Piwi-piRNA pathway. We speculate that the co-option of Nxf2 into TE silencing is not coincidental but may reflect previous TE adaptation to exploit cellular mRNA transport pathways promoting the export of TE transcripts and replication/transposition (Zhang *et al*, 2012; Checkley *et al*, 2013). Why is it necessary for Piwi to use the RNA binding activity of Nxf2 to silence their targets? Piwi, as a member of the Argonaute family, is thought to search for targets through random interactions between Piwi-piRNA and transcripts in the ocean of the transcriptome, many of which likely show partial complementarity with Piwi-loaded piRNAs (Klein *et al*, 2017). To distinguish “scanning Piwi” and “target-engaged Piwi”, the silencing pathway may need an engaged-in system to repress only targets and avoid unnecessary silencing of other cellular transcripts. It is possible that Nxf2 plays a role in supporting the association of Piwi that has found its *bona fide* targets (Appendix Fig S2H). Panx preferentially associates with Piwi, which loads piRNAs targeting TEs (Sienski *et al*, 2015), suggesting that there may be a system for Panx-Nxf2 to form the PPNP complex, specifically with Piwi that is engaged with its target TEs. Our CLIP analysis shows that Nxf2 cannot associate with target TEs without the activity of Piwi (Fig 6), indicating that the Panx-Nxf2-P15 complex itself does not recognize target transcripts, but rather recognizes target-engaged Piwi. In line with this, while piRNA-targeted Piwi can repress the reporter gene (Fig EV3),  $\lambda$ N-tethered Piwi cannot (Fig 3). This may be due to the Panx-Nxf2-p15 complex recognizing only piRNA-directed target-engaged Piwi, but not scanning or  $\lambda$ N-tethered Piwi (Appendix Fig S2H and I). Further studies will be necessary to confirm this speculation and elucidate the precise mechanism by which the Panx-Nxf2-P15 complex selectively recognizes only the “target-engaged Piwi” and forms a PPNP complex to induce silencing of its targets.

## Materials and Methods

### Cell culture and transfection

Ovarian somatic cells (OSCs) were established in the previous studies (Niki *et al*, 2006; Saito *et al*, 2009). Ovarian somatic cells were cultured in Shield and Sang M3 Insect Medium (Sigma) supplemented with 10% fly extract, 10% fetal bovine serum, 0.6 mg/ml glutathione, and 10 µg/ml insulin as described previously. For the transfection of small interfering (si)RNA into OSCs, 40–300 pmol siRNA duplex was nucleofected into  $3.0 \times 10^6$  cells using the Cell Line 96-well Nucleofector Kit SF (Lonza) and program DG150 of the 96-well Shuttle Device (Lonza). The siRNAs were transfected twice for 4-day KD, and once for 2-day KD. The siRNA sequences are listed in Appendix Table S3. Co-transfection of siRNA and plasmid DNA was performed using the Cell Line Nucleofector Kit V (Lonza) and program T-029 of the Nucleofector II Device (Lonza). For immunoprecipitation, expression vectors were transfected using Xfect Transfection Reagent (TaKaRa Clontech), in accordance with the manufacturer's instructions.

### Drosophila strains

Oregon R (OR) was employed as a wild-type strain. Lines harboring shRNA for Nxf2 ( $y[1] \text{ sc}[*] \text{ v}[1]; P\{y[+7.7] \text{ v}[+t1.8] = \text{TRiP.HMS00945}\}attP2/TM3, Sb[1]$ ) and MTD-Gal4 lines ( $P\{w[+mC] = \text{otu-GAL4::VP16.R}\}1, w[*]; P\{w[+mC] = \text{GAL4-nos.NGT}\}40; P\{w[+mC] = \text{GAL4::VP16-nos.UTR}\}CG6325[MVD1]$ ) were obtained from Bloomington *Drosophila* Stock Center (Stock# 33985 and 31777, respectively). For the tethering assay in fly ovary, GFP reporter line ( $If/CyO; tub>EGFP\_5xBoxB\_SV40 [attP2]/TM3, Ser$ ),  $\lambda N$  line as a control ( $pUASp>\lambda\text{mbdaN-HA} [attP40]/CyO; tub>EGFP\_5xBoxB\_SV40 [attP2]/TM3, Ser$ ),  $\lambda N$ -Piwi line ( $pUASp>\lambda\text{mbdaN-HA-Piwi} [attP40]/CyO; tub>EGFP\_5xBoxB\_SV40 [attP2]/TM3, Ser$ ), and  $\lambda N$ -Panx line ( $pUASp>\lambda\text{mbdaN-HA-CG9754} [attP40]/CyO; tub>EGFP\_5xBoxB\_SV40 [attP2]/TM3, Ser$ ) were obtained from Vienna *Drosophila* Resource Center (VDRC) (Stock# 313408, 313390, 313392, and 313393, respectively). All stocks were maintained at 25°C. For calculation of the egg hatching rate, 20 females were mated with Oregon R males in yeasted apple agar plates. The females were left in the plate to continue laying eggs after mating. Laid eggs were counted after 24 h, and hatched eggs were counted after another 24 h.

### Construction of expression plasmids

To produce expression vectors, full-length cDNA was amplified using primers described in Appendix Table S3. First-strand cDNA was synthesized from total RNA isolated from the OR ovaries or OSCs. PCR products were then inserted into the pGEX-5X expression vector (GE Healthcare Bioscience), pET28 expression vector (Novagen), pAcM vector (Saito *et al*, 2006), pAcF vector, or pAcEGFP vector (EGFP cloned into the myc tag region of the pAcM vector), using restriction enzyme cloning or In-Fusion HD Cloning Kit (Clontech) (described in Appendix Table S3). The pGEX-5X or pET28 expression vector was used to express GST- or HIS-fused proteins, and the pAcM, pAcF, or pAcEGFP vector was used to express myc-, Flag-, or EGFP-tagged proteins in OSCs. To yield siRNA-resistant mutants and

mutants for domain mapping experiments, inverse PCR was performed using the described oligonucleotides (Appendix Table S3). The inserted fragment for the pAcF-Nxf2 vector was obtained by HindIII/EcoRI restriction enzyme digestion of the pAcM-Nxf2 vector and ligated into the pAcF vector. Note that plasmid construction for the tethering assay is described in the “Tethering assay using OSCs” and “Tethering assay in fly ovary” sections.

### Production of antibodies (anti-Panx, anti-Nxf2, anti-Eggless, anti-p15)

The middle fragment of the Panx protein (181–361 aa), N-terminal region of the Eggless protein (1–405 aa), or full-length p15 protein (1–134 aa) fused with glutathione S-transferase (GST), and full-length Nxf2 (1–841 aa) fused with histidine (HIS) were used as antigens to immunize mice. The anti-Panx, -Nxf2, and -Eggless monoclonal antibodies were produced essentially as described previously (Ishizuka *et al*, 2002; Saito *et al*, 2006). For the anti-p15 antibody, serum from immunized mice was used for a polyclonal antibody.

### Immunoprecipitation

To obtain whole-cell lysate, OSCs were washed in PBS and lysed in IP buffer (50 mM HEPES-KOH pH 7.4, 200 mM KCl, 1 mM EDTA, 1% Triton X-100, 0.1% Na-deoxycholate or 30 mM HEPES-KOH pH 7.4, 150 mM KOAc, 5 mM MgOAc, 5 mM DTT, 0.1% NP-40) followed by probe-sonication (BRANSON, SFX150, or Bioruptor). After centrifugation, the supernatant was used for immunoprecipitation. To prepare nuclear lysate, OSCs were washed in PBS and suspension buffer (10 mM HEPES-KOH pH 7.4, 10 mM KCl, 1.5 mM MgCl<sub>2</sub>, 0.5 mM DTT) and then homogenized in suspension buffer by passing through a syringe with a 25G needle. After centrifugation, supernatant was recovered as cytoplasmic lysate. The nuclear pellet was washed once and then resuspended in IP buffer, followed by probe-sonication. The nuclear lysate was centrifuged and the supernatant was kept for immunoprecipitation. Antibodies were immunized on Dynabeads Protein G (Thermo Fisher) and incubated with lysates for 1–2 h, at 4°C. Then, beads were washed three to five times in IP buffer. Control immunoprecipitation using mouse nonimmune IgG (IBL) was conducted in parallel.

### Western blotting

Western blotting was performed as described previously (Saito *et al*, 2006). Besides the antibodies generated in this study, anti-Piwi (Saito *et al*, 2006; hybridoma supernatant), anti-DmGTSF1/Arx (Ohtani *et al*, 2013) (hybridoma supernatant), anti-Mael (Sato *et al*, 2011) (hybridoma supernatant), anti-H1 (Iwasaki *et al*, 2016) (hybridoma supernatant), anti-Tubulin (E7, hybridoma supernatant), anti-myc (9E10, hybridoma supernatant), anti-flag (M2, sigma) (1:1,000), anti-H3 (ab1791, Abcam) (1:2,000), anti-HP1a (C1A9, DSHB) (1:1,000), anti-HA (HA-7, Sigma) (1:1,000), and anti-GFP (11814460001, Roche) (1:1,000) antibodies were used.

### Silver staining and mass spectrometry analysis

Silver staining was performed using the SilverQuest Silver Staining Kit (Invitrogen), in accordance with the manufacturer's instructions.



The bands shown in Fig 1A were excised, de-stained, and sent for liquid chromatography–tandem mass spectrometry (MS) analysis to identify the peptides (Support Center for Advanced Medical Sciences, The University of Tokushima, Japan). The results were analyzed using Mascot (Matrix Science), and Scaffold4 (Proteome Software Inc.) was used to validate MS/MS-based peptides.

### Immunofluorescence

Immunofluorescence of OSCs and *Drosophila* ovaries was performed using anti-Panx IgG1 (hybridoma supernatant) or anti-myc (9E10, hybridoma supernatant) antibody as described previously (Ishizuka et al, 2002). Alexa Fluor 546- or 488-conjugated anti-mouse IgG1 (Molecular Probes) (1:1,000 dilution) was used as secondary antibody. Slides were mounted using VECTASHIELD Mounting Medium with DAPI (Vector Laboratories).

### Quantitative reverse-transcription PCR and northern blotting

qRT–PCR analysis and northern blotting were performed as previously described (Iwasaki et al, 2016). Oligonucleotides used for qRT–PCR primers and northern blotting probes are described in Appendix Table S3. Previously described primers (Sienski et al, 2015) were used for qRT–PCR analysis of TE expression levels in ovary.

### Shotgun proteome analysis

Immunoprecipitated proteins were eluted with 100 mM Tris–HCl (pH 8) and 2% sodium dodecyl sulfate (SDS). To remove the SDS from the eluted samples, the methanol–chloroform protein precipitation method was used. Briefly, four volumes of methanol, one volume of chloroform, and three volumes of water were added to the eluted sample and mixed thoroughly. Samples were centrifuged at 20,000 *g* for 10 min, the water phase was carefully removed, and then, four volumes of methanol were added to the samples, followed by centrifugation at 20,400 *g* for 10 min. The supernatant was removed, and the pellet was washed once with 100% ice-cold acetone. Precipitated proteins were re-dissolved in guanidine hydrochloride and reduced with Tris(2-carboxyethyl)phosphine hydrochloride, alkylated with iodoacetamide, and then digested with lysyl endopeptidase and trypsin. Digested peptides were analyzed using a direct nanoflow liquid chromatography system coupled to a time-of-flight mass spectrometer (QSTAR Elite, Sciex). Mass spectrometry and tandem mass spectrometry spectra were obtained in the information-dependent acquisition mode and were queried against the NCBI non-redundant database with an in-house Mascot server (Natsume et al, 2002) (version 2.2.1; Matrix Science).

### Shotgun proteome data analysis

Shotgun proteome was performed in two biological replicates, and two technical replicates per each sample (in total of four measurements per sample). The obtained peptide numbers for four measurements were used to calculate Enrichment and Specificity of obtained protein candidate. Enrichment was calculated by dividing the total number of peptides obtained in Flag-Nxf2-IP samples by control samples, and taking log<sub>2</sub>. Specificity was calculated as *P*-value

obtained from *t*-test of peptide counts obtained for Flag-Nxf2-IP samples against control IP samples.

### EMSA

For EMSA, 16-mer single-stranded RNA (5'-AGCACCGUAAA GACGC-3') described previously (Vourekas et al, 2015) was 5'-end-radiolabelled by p32 and 1 nM was incubated with the indicated amount of GST protein for 15 min at room temperature in 10 μl of RNA binding buffer [50 mM Tris–HCl (pH 7.5), 50 mM KOAc, 2 mM MgCl<sub>2</sub>, 1 mM DTT, and 1 U/μl RNasin]. After incubation, 1 μl of 50 mg/ml heparin was added and incubated for another 10 min, and the reactions were analyzed using 5% native PAGE (Tris-glycine gel) at 4°C. The results were visualized by phospho-imaging.

### Tethering assay using OSCs

We established a tethering assay system in OSCs based on the system in fly ovary, which was reported by Hannon's group (Yu et al, 2015). To obtain firefly luciferase reporter constructs, a 5× boxB fragment was amplified from fly genomic DNA (VDRRC #313408) and cloned into an EcoRI and XhoI sites of pAc5.1B, followed by insertion of luciferase fragment amplified from pCMV-luc at a KpnI and EcoRI site, resulting in pAc-Fluc-5boxB. To obtain pAc-Fluc-10boxB, PCR-amplified 5× boxB carrying a Sall and XhoI site was inserted into a XhoI site of pAc-Fluc-5boxB. To produce pUb-Fluc-10boxB, we replaced the actin 5c promoter of pAc-Fluc-10boxB with a ubiquitin promoter at BglII and KpnI sites. The ubiquitin promoter was amplified from fly genomic DNA. For the intronic boxB reporter construct, we first removed the XhoI site in pAc-Fluc and replaced its actin 5c promoter with the ubiquitin promoter. Subsequently, 5× boxB fragments were inserted twice into the XhoI site within the intron of the ubiquitin promoter. In this process, a reporter construct with 14× boxB in the intron, pUb-14boxB-Fluc, was incidentally obtained, and its sequence was confirmed. For λN-HA fusion protein expression constructs, a λN-HA fragment was amplified from a plasmid, pUASp-λN-Empty (kindly provided by Dr. Brennecke), and inserted into an NheI site of pAcM-based and pAcEGFP-based expression plasmids. The oligonucleotides used for plasmid construction are described in Appendix Table S3.

Isolation of the OSC line carrying reporter gene was performed essentially as described previously (Sumiyoshi et al, 2016). OSCs were co-transfected with a reporter construct and a plasmid carrying a blasticidin-resistance gene, using ScreenFect A (Wako), followed by selection with 25 μg/ml blasticidin for 24 h. Subsequently, 1 × 10<sup>5</sup> cells were passaged in a 6-cm dish and allowed to form colonies in medium supplemented with or without a lower concentration of blasticidin (4–8 μg/ml). Some colonies were isolated and selected using a luciferase assay.

For the tethering assay, 3 × 10<sup>6</sup> OSCs were transfected with 5 μg of plasmid DNA using the Cell Line Nucleofector Kit V (Lonza) and Program T-029 of the Nucleofector II Device (Lonza) and passaged in four wells of a 24-well tissue culture plate. Cells were lysed in 150 μl of 1× Glo Lysis Buffer (Promega). Aliquots of cell lysates were used to measure firefly luciferase activity using ONE-Glo Ex Luciferase Assay system (Promega) and Cytation 5 (BioTek). Total

protein concentration of cell lysates was measured by a Bradford assay (Bio-Rad).

### Tethering assay in fly ovary

Based on previous reports, we carried out a tethering assay in fly ovary (Sienski *et al*, 2015; Yu *et al*, 2015). For the RNA-tethering system in fly ovary, a DNA fragment of myc-Nxf2 was inserted at NheI and EcoRI sites in pUASp- $\lambda$ N-MCS, resulting in pUASp- $\lambda$ N-HA-myc-Nxf2. To obtain pUASp- $\lambda$ N-MCS, a  $\lambda$ N fragment including multiple cloning sites was inserted between KpnI and NotI sites in pUASp- $\lambda$ N-Empty (kindly provided by Dr. Brennecke). Oligonucleotides used for plasmid construction are described in Appendix Table S3. A transgenic line was established by phiC31-mediated integration of pUASp- $\lambda$ N-HA-myc-Nxf2 into the attP40 landing site (Bischof *et al*, 2007; Markstein *et al*, 2008), resulting in a transgenic line (y'w1118;attP40{ $\lambda$ N-HA-myc-Nxf2}/CyO). Transgenic and GFP reporter flies were crossed with a double balancer (Sp/CyO; Pr/TM3, Ser, sb), and then, the progeny were crossed together, resulting in a transgenic line carrying GFP reporter gene and  $\lambda$ N-HA-myc-Nxf2 gene (y'w1118; attP40{ $\lambda$ N-HA-myc-Nxf2}/CyO; tub>EGFP\_5xBoxB\_SV40 [attP2]/TM3). Fly ovaries were fixed in 4% formaldehyde and stained with DAPI, followed by microscopic observation to detect GFP signal in the egg chamber.

### piRNA reporter gene assay

We established a piRNA reporter assay system in OSCs, based on the reports by Lau's group (Post *et al*, 2014). We selected 0.6 kbp and 1.3 kbp flanking elements, from which a number of piRNAs are derived, were cloned into the intron of pUb-Fluc in sense orientation or in antisense orientation relative to the luciferase transcripts. These flanking elements were amplified using primers described in Appendix Table S3. DNA and siRNA transfection, and luciferase assays in OSCs and S2 cells were performed as described in the "Tethering assay using OSCs" section.

### ChIP-qPCR analysis

For ChIP using anti-RNA polymerase II antibody (8WG16; Santa Cruz), OSCs were fixed in 0.3% formaldehyde (methanol-free; Thermo Fisher) and lysed in sonication buffer (50 mM Tris-HCl pH 7.9, 150 mM NaCl, 1 mM EDTA, 1% Triton X-100, 0.1% Na-deoxycholate), followed by probe-sonication (BRANSON, SFX150). After centrifugation, the supernatant was passed through a 0.22- $\mu$ m syringe filter (Membrane Solutions) and used for immunoprecipitation. For ChIP using anti-H1 (Iwasaki *et al*, 2016) (hybridoma supernatant), anti-H3K9me3 (0319, Active motif), and anti-H3K4me3 (ab8580, Abcam), OSCs were fixed in 1% formaldehyde and lysed in ChIP buffer (50 mM Tris-HCl pH 7.9, 5 mM EDTA, 0.1% SDS), followed by probe-sonication. After centrifugation, the supernatant was mixed with dilution buffer (50 mM Tris-HCl pH 7.9, 250 mM NaCl, 1.6% Triton X-100, 0.16% Na-deoxycholate), passed through a 0.22- $\mu$ m syringe filter, and used for immunoprecipitation. Lysates were incubated with antibodies on Dynabeads Protein G for 3 h, at 4°C. Beads were washed in a series of wash buffers: low-salt wash buffer (20 mM Tris-HCl pH 7.9, 150 mM NaCl, 2 mM EDTA, 1%

Triton X-100, 0.1% Na-deoxycholate), high-salt wash buffer (20 mM Tris-HCl pH 7.9, 500 mM NaCl, 2 mM EDTA, 1% Triton X-100, 0.1% Na-deoxycholate), LiCl wash buffer (10 mM Tris-HCl pH 7.9, 250 mM LiCl, 1 mM EDTA, 1% NP-40, 0.5% Na-deoxycholate), and TE (10 mM Tris-HCl pH 7.9, 1 mM EDTA). Protein-DNA complexes were eluted from beads in elute buffer (50 mM Tris-HCl pH 7.9, 10 mM EDTA, 1% SDS) at 65°C for 10 min, followed by reversing cross-linking at 65°C for over 12 h in the presence of 200 mM NaCl. DNA was recovered and quantified with the Dice Real Time System III (TaKaRa) using TB Green Fast qPCR Mix (TaKaRa) and primer sets for the reporter gene (described in Appendix Table S3).

### mRNA-seq analysis

Preparation and sequencing of Poly(A)<sup>+</sup> RNA libraries and computational analyses were performed as described previously (Iwasaki *et al*, 2016). Libraries were prepared from total RNA obtained from OSCs with 4-day knockdown of the indicated genes and analyzed by Illumina HiSeq. This yielded 10–17 million reads per sample. For computational analysis of the obtained reads, Bowtie 2.2.9 (Langmead & Salzberg, 2012) was used with the default parameters to map sequences to the *Drosophila* genome (dm3). Reads mapped to the genome were then mapped to the *Drosophila melanogaster* TE consensus sequence from Repbase (Jurka, 1998), using Bowtie 1.0.1, and those that were uniquely mapped were extracted. Expression levels (RPKM) of TEs were calculated using reads that were mapped to the TE consensus sequence. Expression levels (RPKM) of coding genes were calculated using TopHat 2.0.14 (Trapnell *et al*, 2009) and DESeq2 (Love *et al*, 2014). *Drosophila melanogaster* (dm3) GTF files obtained from Illumina iGenomes were used to define known gene structures. Analysis of coding genes was performed using duplicate samples. Duplicate data were obtained for EGFP-, Nxf2-, and Panx-KD samples, and previously published data (Iwasaki *et al*, 2016) were used as duplicate data for Piwi-KD samples.

### ChIP-seq analysis

ChIP was performed as described previously (Iwasaki *et al*, 2016). Briefly, OSCs ( $3 \times 10^7$ ) were fixed and lysed, and their nuclei were isolated using truChIP Chromatin Shearing Kits (Covaris), in accordance with the manufacturer's instructions. Sodium deoxycholate was added to a final concentration of 0.4% prior to shearing. DNA was sonicated to ~300 bases using Bioruptor (Cosmobio) and then diluted with ChIP buffer [1  $\times$  50 mM HEPES-KOH pH 7.4, 150 mM NaCl, 1 mM EDTA, 1% Triton X-100, Halt Protease Inhibitor Cocktail (Thermo Scientific)]. DNA-protein complexes were incubated with 3  $\mu$ g of anti-H3K9me3 antibody (61013; Active Motif) on Dynabeads Protein G for 4 h, at 4°C. Beads were washed with ChIP buffer, high-salt lysis buffer (50 mM HEPES-KOH pH 7.4, 450 mM NaCl, 1 mM EDTA, 1% Triton X-100, 0.1% SDS), and wash buffer (50 mM Tris-HCl pH 8.0, 1 mM EDTA, 250 mM lithium chloride, 0.5% NP-40, 0.5% SDS) followed by TE (10 mM Tris-HCl pH 8.0, 1 mM EDTA). After reversing cross-linking for 12–16 h at 65°C, samples were treated with RNase for 30 min at 37°C and Proteinase K for 60 min at 55°C. DNA was then recovered. To prepare ChIP-seq libraries, DNA fragments from the ChIP experiment were sheared to ~200 bases using Covaris S220 (Covaris). These were

used for library preparation with the NEBNext Ultra DNA Library Prep Kit for Illumina II (NEB), following the manufacturer's protocol. ChIP-seq libraries were sequenced with Illumina MiSeq using MiSeq Reagent Kit v3 for 150 cycles (Illumina). For ChIP-seq analysis, adapters were removed from the reads using Cutadapt, and subsequent reads shorter than 50 nt were discarded. ChIP-seq reads were mapped to the *Drosophila* genome (dm3) using Bowtie 1.0.1 (Langmead *et al*, 2009), using -v 2 -best parameters. Reads mapped to the genome were extracted and mapped to *Drosophila melanogaster* TE consensus sequences from Repbase (Jurka, 1998), permitting only those that mapped uniquely to the TE consensus sequence. Metaplots of ChIP signals were calculated using ngs.plot (Shen *et al*, 2014). Coordinates of TE insertions and the euchromatin/heterochromatin distribution within OSCs were obtained from a previous publication (Sienski *et al*, 2012). For peak calling of H3K9me3 signals, MACS-1.4.2 (Zhang *et al*, 2008) was used with the default parameters. ChIP-seq analysis was performed in duplicates for Panx and Nxf2 4-day knockdown samples, and EGFP (control) and Piwi 4-day knockdown samples were obtained from a previous study (Iwasaki *et al*, 2016).

#### CLIP-seq

For the preparation of preadenylated 3' adapter, DNA oligonucleotide (5'-/5phos/TGGAATTCTCGGGTGCCAAGG/3Bio/-3';/5' phos/= 5' phosphorylation,/3' Bio/= 3' biotin) was custom-synthesized by IDT and then preadenylated using the 5' DNA Adenylation Kit (NEB) following the manufacturer's protocol. The reaction was ethanol-precipitated and dissolved in water to a final concentration of 20  $\mu$ M. cDNA synthesis primer (5'-/5phos/NNAACNNNGATCGTCCGACTGTAGAACTCTGAA/iSp18/CACTCA/iSp18/ATCTCCTTGGCACCCGAGAATTCCA-3';/iSp18/= Carbon-18 spacer) and Illumina sequencing primers [RP1: AATGATACGGC GACCACCGAGATCTACACGTTACAGATTCTACAGTCCGA, RPIx: C AAGCAGAAGACGGCATAACGAGATXXXXXGTGACTGGAGTTCCTT GGCACCCGAGAATTCCA, 6-bases index sequence in bold (see Illumina customer service letter for other index sequences)] were custom-synthesized by IDT.

The iCLIP libraries were prepared as previously described (Flynn *et al*, 2015; Van Nostrand *et al*, 2016) with the following modifications. For iCLIP from stable cell line of myc-Nxf2, three confluent 15-cm plates (Nunc) per replicate were used. Cells were UV-cross-linked with irradiance of 200 mJ/cm<sup>2</sup> at 254 nm using UV Stratalinker 1800 (Stratagene). Cells were harvested and lysed with 2 ml of lysis buffer [20 mM HEPES-KOH (pH7.3), 150 mM NaCl, 1 mM EDTA, 1 mM DTT, 0.5% NP-40, 2  $\mu$ g/ml pepstatin, 2  $\mu$ g/ml leupeptin, 0.5% aprotinin]. Cell extracts were treated with 1 U/ $\mu$ l RNase T1 (Roche) for 15 min at room temperature. The lysate was cleared by centrifugation at 16,500 g for 15 min at 4°C. The resulting supernatant was then collected and cooled on ice. 10  $\mu$ l was reserved for size-matched input (SMInput; Van Nostrand *et al*, 2016). RNA-protein complexes were immunoprecipitated using 40  $\mu$ g of mouse monoclonal antibodies (anti-myc 9E10, DSHB) and 200  $\mu$ l of Protein G Dynabeads (Invitrogen) for 2 h, at 4°C. Beads were then washed three times with IP wash buffer [20 mM HEPES-KOH (pH7.3), 300 mM NaCl, 1 mM DTT, 0.05% NP-40, 2  $\mu$ g/ml pepstatin, 2  $\mu$ g/ml leupeptin, 0.5% aprotinin] and three times with high-salt wash buffer [20 mM HEPES-KOH (pH7.3), 500 mM NaCl,

1 mM DTT, 0.05% NP-40, 2  $\mu$ g/ml pepstatin, 2  $\mu$ g/ml leupeptin, 0.5% aprotinin]. Washed beads were resuspended in 30  $\mu$ l of 1 $\times$ NuPAGE LDS sample buffer (Thermo Fisher) with 50 mM DTT and incubated at 70°C for 10 min. Released RNA-protein complexes were separated on the 4–12% NuPAGE Bis-Tris gel (Thermo Fisher) with MOPS running buffer (Thermo Fisher) at 200 V for 1 h. After the run, RNA-protein complexes from the gel were transferred to a nitrocellulose membrane using the Novex wet transfer apparatus following the manufacturer's protocol (Thermo Fisher). The transfer was performed for 1 h at 30 V using NuPAGE transfer buffer (Thermo Fisher). Western blotting was performed using SNAP i.d. 2.0 System (Merck) following the manufacturer's instruction to visualize bands and determine regions for isolating RNA-protein complexes. Briefly, the membrane was blocked with 0.5% skim milk in PBS-0.1% Tween-20, incubated with 1:1,000 anti-myc antibody, washed with PBS-0.1% Tween-20, and incubated with 1:5,000 HRP-conjugated secondary antibody (Cappel). Membranes were developed with ECL substrate (GE) and exposed using film. A region 50 kDa above the protein size was cut into 1- to 2-mm-narrow strips and then transferred to a 1.5-mL tube. To each tube, 200  $\mu$ l of Proteinase K buffer [100 mM Tris-HCl (pH 7.5), 150 mM NaCl, 12.5 mM EDTA, 2% (w/v) SDS] and 10  $\mu$ l of Proteinase K (Roche) were added and incubated for 30 min at 55°C. The RNA was recovered by acidic phenol/chloroform extraction followed by a chloroform extraction and an ethanol precipitation with Pellet Paint NF Co-Precipitant (Merck Millipore). Finally, the pellet was dissolved in 16  $\mu$ l of nuclease-free water. The recovered RNA was mixed with dephosphorylation mix [2  $\mu$ l of 10  $\times$  PNK buffer pH 6.0 (500 mM imidazole-HCl pH 6.0, 100 mM MgCl<sub>2</sub>, 50 mM DTT), 1  $\mu$ l of RNasin (Promega), 1  $\mu$ l of T4 PNK (NEB)] and incubated for 30 min at 37°C. The sample was incubated with 10  $\mu$ l of SPRIselect (Beckman Coulter) and 30  $\mu$ l of isopropanol for 5 min and then separated on the magnetic stand for 5 min. The supernatant was discarded, and the beads were washed twice with 500  $\mu$ l of 85% ethanol. The beads were then air dried for 5 min and eluted with 10.2  $\mu$ l of nuclease-free water. The recovered RNA was mixed with 3' adapter ligation mix (1  $\mu$ l of 20  $\mu$ M preadenylated 3' adapter, 2  $\mu$ l of 10  $\times$  T4 RNA ligase buffer, 4.8  $\mu$ l of 50% PEG8000, 1  $\mu$ l of RNasin, 1  $\mu$ l of T4 RNA ligase2, truncated KQ (NEB)) and incubated overnight at 16°C. Ligation products were purified using 10  $\mu$ l of SPRIselect and 10  $\mu$ l of isopropanol in the same procedure as above, and eluted with 16  $\mu$ l of nuclease-free water. The sample was mixed with 5' deadenylation mix (2  $\mu$ l of 10  $\times$  NEB2 buffer, 1  $\mu$ l of RNasin, 1  $\mu$ l of 5' Deadenylase (NEB)) and incubated 30 min at 30°C. To digest unligated adapters, 5  $\mu$ l of RecJf exonuclease (NEB) was added and incubated 30 min at 37°C. Ligation products were purified using 12.5  $\mu$ l of SPRIselect and 12.5  $\mu$ l of isopropanol in the same procedure as above, and eluted with 12.2  $\mu$ l of nuclease-free water. 1  $\mu$ l of 10  $\mu$ M cDNA synthesis primer was added to the whole isolated RNA and annealed to the adapter by incubation at 70°C for 5 min and at 25°C for 1 min. RT mix [4  $\mu$ l of 5  $\times$  Superscript III RT buffer, 0.8  $\mu$ l of dNTP mix (10 mM each), 1  $\mu$ l of 0.1 M DTT, 1  $\mu$ l of Superscript III RT (Thermo Fisher)] was added, and a reverse transcription reaction was performed using the following program: 42°C for 40 min, 50°C for 15 min, and 4°C for hold. After reverse transcription reaction, 0.5  $\mu$ l of RNase (Roche) and 0.5  $\mu$ l of RNaseH (NEB) were added to each sample and incubated at 37°C for 15 min. During this time, 5  $\mu$ l of Dynabeads M-270 Streptavidin

(Invitrogen) was washed twice with 200  $\mu$ l of StrepBead wash buffer (100 mM Tris-HCl, pH 7, 1 M NaCl, 10 mM EDTA, 0.1% Tween-20), for each sample. Each 5  $\mu$ l volume of beads was finally resuspended in 40  $\mu$ l of StrepBead wash buffer. After RNase digestion, 40  $\mu$ l of pre-washed beads was added to each sample and incubated at 25°C for 30 min with rotation. After incubating, the samples were applied to a magnetic stand and the buffer was discarded. Each sample was washed four times with 100  $\mu$ l of wash buffer (100 mM Tris-HCl pH 7, 4 M NaCl, 10 mM EDTA, 0.2% Tween-20) and twice with 100  $\mu$ l of NT2 buffer (50 mM Tris-HCl, pH 7.5, 150 mM NaCl, 1 mM MgCl<sub>2</sub>, 0.05% NP-40). The purified cDNA was then circularized by adding 20  $\mu$ l of CircLigase Reaction Mix (2  $\mu$ l of 10  $\times$  CircLigaseII Reaction Buffer, 1  $\mu$ l of 50 mM MnCl<sub>2</sub>, 1  $\mu$ l of CircLigaseII ssDNA Ligase (Epicentre), 16  $\mu$ l of nuclease-free water) to each sample, and incubating for 1 h at 60°C, 10 min at 80°C, and hold at 4°C. Samples were then applied to a magnetic stand, the reaction buffer was collected (be sure not to discard the reaction buffer), and another 20  $\mu$ l of elution buffer (10 mM Tris pH 7.5 and 1  $\mu$ M PR1x primer) was added to the beads and heated at 95°C for 2 min. Samples were then applied to a magnetic stand and the elution buffer was removed and combined with reaction buffer, collected earlier (20  $\mu$ l). The elution was repeated for two times in total obtaining a final volume of 60  $\mu$ l. cDNA was purified using 30  $\mu$ l of SPRIselect and 60  $\mu$ l of isopropanol in the same procedure as above, and eluted with 29.5  $\mu$ l of nuclease-free water. PCR mix [2.5  $\mu$ l of 10  $\mu$ M RP1 primer, 2.5  $\mu$ l of 10  $\mu$ M RP1x primer, 10  $\mu$ l of 5  $\times$  Q5 Reaction Buffer, 5  $\mu$ l of dNTP mix (2 mM each), 0.5  $\mu$ l of Q5 DNA Polymerase (NEB)] was added to the cDNA, and PCR was performed using the following program: 98°C for 30 s; cycles of 98°C for 10 s, 60°C for 30 s, and 72°C for 15 s, followed by 4°C hold). DNA was amplified with 10 and 12 cycles of PCR for SMInput samples and immunoprecipitated samples, respectively. Amplified DNA was captured with 1.8 volumes of AMPure XP beads (Beckman Coulter) following the manufacturer's protocol and size-selected on 6% PAGE gels. DNA was visualized with SybrGold (Thermo Fisher), and those with sizes between 170 and 200 bp were isolated. The PAGE gel was crushed, and the DNA was eluted in 400  $\mu$ l of 0.4 M NaCl at 4°C on rotation overnight. The eluted DNA was ethanol-precipitated with Pellet Paint NF Co-Precipitant and then re-amplified with the same PCR program and for 8 cycles each. PCR products were captured with 1.8 volumes of AMPure XP beads, size-selected on 6% PAGE gels, and purified as described above. 1  $\mu$ l of libraries was quantitated by HS-DNA Bioanalyzer. Libraries were sequenced on the Illumina Miseq platform.

For Piwi iCLIP from OSCs, one confluent 10-cm plate per replicate was used. Cells were lysed in 1 ml of lysis buffer, and immunoprecipitation was performed using 10  $\mu$ g of anti-Piwi antibody and 50  $\mu$ l of Protein G Dynabeads. The rest of the protocol was identical to that of myc-Nxf2.

### Isolation of myc-Nxf2 stable line OSCs

Myc-Nxf2 OSC line was isolated using the methodology described in "Tethering assay using OSCs" section, for isolation of OSC line carrying reporter gene. Briefly, OSCs were co-transfected with pAcM-Nxf2-sires plasmid and the plasmid carrying a blasticidin-resistant gene, and selection was performed by blasticidin.

### Small RNA-seq analysis

Small RNA cloning was performed as previously described (Iwasaki et al, 2017), with modifications. In summary, co-immunoprecipitated piRNA was extracted from Piwi immunoprecipitates using phenol and chloroform, and purified piRNAs were cloned using the NEXTflex Small RNA Sequencing kit v3 (NEXTflex). The libraries were analyzed on a Miseq platform (Illumina).

For small RNA-seq data analysis, 4 nt random nucleotides and adapter sequences were removed from the obtained reads using Cutadapt, and reads out of 20–35 nt size range were removed for further analysis. Obtained reads were mapped to the Release 3 assembly of the *Drosophila* genome using Bowtie (Langmead et al, 2009), allowing up to single mismatch. Genome-mapped reads were further mapped to TE consensus sequences from Repbase (Jurka, 1998) using Bowtie (Langmead et al, 2009), allowing no mismatch and unique mapping. The reads were normalized to RPM by the number of *Drosophila* genome-mapped reads. Reads mapped to anti-sense direction of TE consensus sequences were used to generate heatmap in Fig 6E, and reads mapped to both directions were used to generate density plot in Fig 6F. Sense reads were plotted in positive direction, where antisense reads were plotted in negative direction.

### CLIP-seq data analysis

First, we trimmed 3' adapter sequences using Cutadapt and discarded reads shorter than 27 bp. Next, we removed PCR duplicates by collapsing all identical reads containing the same random barcode at the 5' end with fastx-collapser from the FASTX-Toolkit ([http://hanonlab.cshl.edu/fastx\\_toolkit/index.html](http://hanonlab.cshl.edu/fastx_toolkit/index.html)). Finally, we trimmed the 5'-end random barcode located at positions 1–9 of the reads. Mapping was then performed against the Release 3 assembly of the *Drosophila melanogaster* genome with STAR (Dobin et al, 2013). Alignment output BAM files were sorted and indexed by SAMtools (Li et al, 2009). Peaks were called using Piranha peak-calling algorithm (Uren et al, 2012), and reads within the peaks were counted for two replicate samples. Of two replicate samples, peak position of the sample that had higher number of annotated peaks was used for counting reads. Dot plots were generated based on the read counts, and correlation coefficient (*r*) was calculated to check for the reproducibility (shown in Fig EV6E). After checking for reproducibility, samples were merged for downstream analysis using SAMtools (Li et al, 2009). Genome-mapped reads were further mapped to TE consensus sequences from Repbase (Jurka, 1998) using Bowtie allowing only unique mapping reads. Mapped reads were counted for each consensus TE and normalized to RPM by the number of *Drosophila* genome-mapped reads. Reads mapped to sense and antisense direction of TE consensus sequences were counted separately, when calculating RPM. Based on the results shown in Figs 6A–C and EV6F, sense-mapped read counts were used for analysis shown in Fig 6D–F. Note that piRNAs were not included in the reads mapped to antisense direction of TEs, since the libraries were generated using RNA in the size range of 43–73 nt (~50 kDa above the protein size). In case of taking ratio of CLIP tags and SMInput, TEs that had RPM lower than 0.5 in SMInput were eliminated. Maximum x-axis for the density plot of Piwi CLIP tags in *mdg1* (Fig 6F) was adjusted to 100, since there was single high peak at position 6,870 bp (~600 RPM), which masks



the other peaks. Dot plot, boxplot, and density plot were generated using the methodology described in “RNA-seq” and “ChIP-seq” section. Heatmaps were depicted using Java Treeview (Saldanha, 2004). Transcriptome-wide CLIP data are available at NCBI-GEO, accession number GSE131950.

## Data availability

The datasets produced in this study are available in the following database: RNA-seq, ChIP-seq, CLIP-seq, and small RNA-seq data: Gene Expression Omnibus GSE131950 (<https://www.ncbi.nlm.nih.gov/geo/query/acc.cgi?acc=GSE131950>).

**Expanded View** for this article is available online.

## Acknowledgements

We thank Wataru Ito for experimental support and critical discussions. We also thank Julius Brennecke for sharing plasmids; Kazumichi Nishida, Ryo Ohnishi, and Tatsuki Kinoshita for sharing protocols; and Soichiro Yamanaka for critical reading of the paper. This work was supported by funding from JSPS KAKENHI Grant Number 17K08644 and Kato Memorial Bioscience Foundation to K.M.; from JSPS KAKENHI Grant Numbers 15H05583, 17H05603, 18H02421, and 19H05268, Senri Life Science Foundation, NOVARTIS Foundation (Japan), and the Naito Foundation to Y.W.I.; from JSPS KAKENHI Grant Number 17H05610 to S.A.; from Takeda Science Foundation to T.N.; and from JSPS KAKENHI Grant Number 25221003 to H.S.

## Author Contributions

KM and YWI designed and performed most of the experiments with HI, AM, and AS, SK and KS generated mutant flies for tethering assays, SA and TN performed LC-MS/MS analysis, and SS and MCS generated Eggless antibody. YWI and HS conceived the study, and KM, YWI, and HS wrote the paper with input from the other authors.

## Conflict of interest

The authors declare that they have no conflict of interest.

## References

- Baron-Benhamou J, Gehring NH, Kulozik AE, Hentze MW (2004) Using the lambda<sub>da</sub>N peptide to tether proteins to RNAs. *Methods Mol Biol* 257: 135–154
- Batki J, Schnabl J, Wang J, Handler D, Andreev VI, Stieger CE, Novatchkova M, Lampersberger L, Kauneckaitė K, Xie W *et al* (2019) The nascent RNA binding complex SFINX licenses piRNA-guided heterochromatin formation. *Nat Struct Mol Biol* 26: 720–731
- Bischof J, Maeda RK, Hediger M, Karch F, Basler K (2007) An optimized transgenesis system for *Drosophila* using germ-line-specific phiC31 integrases. *Proc Natl Acad Sci USA* 104: 3312–3317
- Bjork P, Wieslander L (2014) Mechanisms of mRNA export. *Semin Cell Dev Biol* 32: 47–54
- Brennecke J, Aravin AA, Stark A, Dus M, Kellis M, Sachidanandam R, Hannon GJ (2007) Discrete small RNA-generating loci as master regulators of transposon activity in *Drosophila*. *Cell* 128: 1089–1103
- Brower-Toland B, Findley SD, Jiang L, Liu L, Yin H, Dus M, Zhou P, Elgin SCR, Lin HF (2007) *Drosophila* PIWI associates with chromatin and interacts directly with HP1a. *Genes Dev* 21: 2300–2311
- Carmell MA, Girard A, van de Kant HJ, Bourc'his D, Bestor TH, de Rooij DG, Hannon GJ (2007) MIWI2 is essential for spermatogenesis and repression of transposons in the mouse male germline. *Dev Cell* 12: 503–514
- Checkley MA, Mitchell JA, Eizenstat LD, Lockett SJ, Garfinkel DJ (2013) Ty1 gag enhances the stability and nuclear export of Ty1 mRNA. *Traffic* 14: 57–69
- Chen FX, Woodfin AR, Gardini A, Rickels RA, Marshall SA, Smith ER, Shiekhattar R, Shilatifard A (2015) PAF1, a molecular regulator of promoter-proximal pausing by RNA polymerase II. *Cell* 162: 1003–1015
- Chuong EB, Elde NC, Feschotte C (2017) Regulatory activities of transposable elements: from conflicts to benefits. *Nat Rev Genet* 18: 71–86
- Clark JP, Rahman R, Yang N, Yang LH, Lau NC (2017) *Drosophila* PAF1 modulates PIWI/piRNA silencing capacity. *Curr Biol* 27: 2718–2726.e4
- Cox DN, Chao A, Baker J, Chang L, Qiao D, Lin H (1998) A novel class of evolutionarily conserved genes defined by piwi are essential for stem cell self-renewal. *Genes Dev* 12: 3715–3727
- Czech B, Preall JB, McGinn J, Hannon GJ (2013) A transcriptome-wide RNAi screen in the *Drosophila* ovary reveals factors of the germline piRNA pathway. *Mol Cell* 50: 749–761
- Dobin A, Davis CA, Schlesinger F, Drenkow J, Zaleski C, Jha S, Batut P, Chaisson M, Gingeras TR (2013) STAR: ultrafast universal RNA-seq aligner. *Bioinformatics* 29: 15–21
- Donertas D, Sienski G, Brennecke J (2013) *Drosophila* Gtsf1 is an essential component of the Piwi-mediated transcriptional silencing complex. *Genes Dev* 27: 1693–1705
- Ernst C, Odom DT, Kutter C (2017) The emergence of piRNAs against transposon invasion to preserve mammalian genome integrity. *Nat Commun* 8: 1411
- Fabry MH, Ciabrelli F, Munafò M, Eastwood EL, Kneuss E, Falciatori I, Falconio FA, Hannon GJ (2019) piRNA-guided co-transcriptional silencing coopts nuclear export factors. *eLife* 8: e47999
- Flynn RA, Martin L, Spitale RC, Do BT, Sagan SM, Zarnegar B, Qu K, Khavari PA, Quake SR, Sarnow P *et al* (2015) Dissecting noncoding and pathogen RNA-protein interactomes. *RNA* 21: 135–143
- Fribourg S, Braun IC, Izaurralde E, Conti E (2001) Structural basis for the recognition of a nucleoporin FG repeat by the NTF2-like domain of the TAP/p15 mRNA nuclear export factor. *Mol Cell* 8: 645–656
- Gramates LS, Marygold SJ, Santos GD, Urbano JM, Antonazzo G, Matthews BB, Rey AJ, Tabone CJ, Crosby MA, Emmert DB *et al* (2017) FlyBase at 25: looking to the future. *Nucleic Acids Res* 45: D663–D671
- Guang S, Bochner AF, Burkhart KB, Burton N, Pavelec DM, Kennedy S (2010) Small regulatory RNAs inhibit RNA polymerase II during the elongation phase of transcription. *Nature* 465: 1097–1101
- Gunawardane LS, Saito K, Nishida KM, Miyoshi K, Kawamura Y, Nagami T, Siomi H, Siomi MC (2007) A slicer-mediated mechanism for repeat-associated siRNA 5' end formation in *Drosophila*. *Science* 315: 1587–1590
- Han JS, Boeke JD (2005) LINE-1 retrotransposons: modulators of quantity and quality of mammalian gene expression? *BioEssays* 27: 775–784
- Han BW, Wang W, Li C, Weng Z, Zamore PD (2015) Noncoding RNA piRNA-guided transposon cleavage initiates Zucchini-dependent, phased piRNA production. *Science* 348: 817–821
- Handler D, Meixner K, Pizka M, Lauss K, Schmied C, Gruber FS, Brennecke J (2013) The genetic makeup of the *Drosophila* piRNA pathway. *Mol Cell* 50: 762–777
- Herold A, Suyama M, Rodrigues JP, Braun IC, Kutay U, Carmo-Fonseca M, Bork P, Izaurralde E (2000) TAP (NXF1) belongs to a multigene family of putative RNA export factors with a conserved modular architecture. *Mol Cell Biol* 20: 8996–9008



- Herold A, Klymenko T, Izaurralde E (2001) NXF1/p15 heterodimers are essential for mRNA nuclear export in *Drosophila*. *RNA* 7: 1768–1780
- Herold A, Teixeira L, Izaurralde E (2003) Genome-wide analysis of nuclear mRNA export pathways in *Drosophila*. *EMBO J* 22: 2472–2483
- Homolka D, Pandey RR, Goriaux C, Brassat E, Vaury C, Sachidanandam R, Fauvarque MO, Pillai RS (2015) PIWI slicing and RNA elements in precursors instruct directional primary piRNA biogenesis. *Cell Rep* 12: 418–428
- Houwing S, Kamminga LM, Berezikov E, Cronembold D, Girard A, van den Elst H, Filippov DV, Blaser H, Raz E, Moens CB et al (2007) A role for Piwi and piRNAs in germ cell maintenance and transposon silencing in Zebrafish. *Cell* 129: 69–82
- Huang XA, Yin H, Sweeney S, Raha D, Snyder M, Lin H (2013) A major epigenetic programming mechanism guided by piRNAs. *Dev Cell* 24: 502–516
- Ishizuka A, Siomi MC, Siomi H (2002) A *Drosophila* fragile X protein interacts with components of RNAi and ribosomal proteins. *Genes Dev* 16: 2497–2508
- Iwasaki YW, Siomi MC, Siomi H (2015) PIWI-interacting RNA: its biogenesis and functions. *Annu Rev Biochem* 84: 405–433
- Iwasaki YW, Murano K, Ishizu H, Shibuya A, Iyoda Y, Siomi MC, Siomi H, Saito K (2016) Piwi modulates chromatin accessibility by regulating multiple factors including histone H1 to repress transposons. *Mol Cell* 63: 408–419
- Iwasaki YW, Ishino K, Siomi H (2017) Deep sequencing and high-throughput analysis of PIWI-associated small RNAs. *Methods* 126: 66–75
- Izaurralde E (2002) A novel family of nuclear transport receptors mediates the export of messenger RNA to the cytoplasm. *Eur J Cell Biol* 81: 577–584
- Jin Z, Flynt AS, Lai EC (2013) *Drosophila* piwi mutants exhibit germline stem cell tumors that are sustained by elevated Dpp signaling. *Curr Biol* 23: 1442–1448
- Jurka J (1998) Repeats in genomic DNA: mining and meaning. *Curr Opin Struct Biol* 8: 333–337
- Kerkow DE, Carmel AB, Menichelli E, Ambrus G, Hills RD Jr, Gerace L, Williamson JR (2012) The structure of the NXF2/NXT1 heterodimeric complex reveals the combined specificity and versatility of the NTF2-like fold. *J Mol Biol* 415: 649–665
- Klein M, Chandradoss SD, Depken M, Joo C (2017) Why argonaute is needed to make microRNA target search fast and reliable. *Semin Cell Dev Biol* 65: 20–28
- Klenov MS, Lavrov SA, Korbut AP, Stolyarenko AD, Yakushev EY, Reuter M, Pillai RS, Gvozdev VA (2014) Impact of nuclear Piwi elimination on chromatin state in *Drosophila melanogaster* ovaries. *Nucleic Acids Res* 42: 6208–6218
- Kowalik KM, Shimada Y, Flury V, Stadler MB, Batki J, Buhler M (2015) The Paf1 complex represses small-RNA-mediated epigenetic gene silencing. *Nature* 520: 248–252
- Langmead B, Trapnell C, Pop M, Salzberg SL (2009) Ultrafast and memory-efficient alignment of short DNA sequences to the human genome. *Genome Biol* 10: R25
- Langmead B, Salzberg SL (2012) Fast gapped-read alignment with Bowtie 2. *Nat Methods* 9: 357–359
- Le Thomas A, Rogers AK, Webster A, Marinov GK, Liao SE, Perkins EM, Hur JK, Aravin AA, Toth KF (2013) Piwi induces piRNA-guided transcriptional silencing and establishment of a repressive chromatin state. *Genes Dev* 27: 390–399
- Levesque L, Guzik B, Guan T, Coyle J, Black BE, Rekosh D, Hammarskjöld ML, Paschal BM (2001) RNA export mediated by tap involves NXT1-dependent interactions with the nuclear pore complex. *J Biol Chem* 276: 44953–44962
- Li H, Handsaker B, Wysoker A, Fennell T, Ruan J, Homer N, Marth G, Abecasis G, Durbin R, Genome Project Data Processing S (2009) The sequence alignment/Map format and SAMtools. *Bioinformatics* 25: 2078–2079
- Lin H, Spradling AC (1997) A novel group of pumilio mutations affects the asymmetric division of germline stem cells in the *Drosophila* ovary. *Development* 124: 2463–2476
- Love MI, Huber W, Anders S (2014) Moderated estimation of fold change and dispersion for RNA-seq data with DESeq2. *Genome Biol* 15: 550
- Markstein M, Pitsouli C, Villalta C, Celniker SE, Perrimon N (2008) Exploiting position effects and the gypsy retrovirus insulator to engineer precisely expressed transgenes. *Nat Genet* 40: 476–483
- Mohn F, Handler D, Brennecke J (2015) Noncoding RNA: piRNA-guided slicing specifies transcripts for Zucchini-dependent, phased piRNA biogenesis. *Science* 348: 812–817
- Muerdter F, Guzzardo PM, Gillis J, Luo Y, Yu Y, Chen C, Fekete R, Hannon GJ (2013) A genome-wide RNAi screen draws a genetic framework for transposon control and primary piRNA biogenesis in *Drosophila*. *Mol Cell* 50: 736–748
- Natsume T, Yamauchi Y, Nakayama H, Shinkawa T, Yanagida M, Takahashi N, Isobe T (2002) A direct nanoflow liquid chromatography-tandem mass spectrometry system for interaction proteomics. *Anal Chem* 74: 4725–4733
- Niki Y, Yamaguchi T, Mahowald AP (2006) Establishment of stable cell lines of *Drosophila* germ-line stem cells. *Proc Natl Acad Sci USA* 103: 16325–16330
- Ohtani H, Iwasaki YW, Shibuya A, Siomi H, Siomi MC, Saito K (2013) DmGTSF1 is necessary for Piwi-piRISC-mediated transcriptional transposon silencing in the *Drosophila* ovary. *Genes Dev* 27: 1656–1661
- Post C, Clark JP, Sytnikova YA, Chirn GW, Lau NC (2014) The capacity of target silencing by *Drosophila* PIWI and piRNAs. *RNA* 20: 1977–1986
- Rozhkov NV, Hammell M, Hannon GJ (2013) Multiple roles for Piwi in silencing *Drosophila* transposons. *Genes Dev* 27: 400–412
- Saito K, Nishida KM, Mori T, Kawamura Y, Miyoshi K, Nagami T, Siomi H, Siomi MC (2006) Specific association of Piwi with rasiRNAs derived from retrotransposon and heterochromatic regions in the *Drosophila* genome. *Genes Dev* 20: 2214–2222
- Saito K, Inagaki S, Mituyama T, Kawamura Y, Ono Y, Sakota E, Kotani H, Asai K, Siomi H, Siomi MC (2009) A regulatory circuit for piwi by the large Maf gene traffic jam in *Drosophila*. *Nature* 461: 1296–1299
- Saito K, Ishizu H, Komai M, Kotani H, Kawamura Y, Nishida KM, Siomi H, Siomi MC (2010) Roles for the Yb body components Armitage and Yb in primary piRNA biogenesis in *Drosophila*. *Genes Dev* 24: 2493–2498
- Saldanha AJ (2004) Java Treeview—extensible visualization of microarray data. *Bioinformatics* 20: 3246–3248
- Sato K, Nishida KM, Shibuya A, Siomi MC, Siomi H (2011) Maelstrom coordinates microtubule organization during *Drosophila* oogenesis through interaction with components of the MTOC. *Genes Dev* 25: 2361–2373
- Shen L, Shao N, Liu X, Nestler E (2014) ngs.plot: Quick mining and visualization of next-generation sequencing data by integrating genomic databases. *BMC Genom* 15: 284
- Sienski G, Donertas D, Brennecke J (2012) Transcriptional silencing of transposons by Piwi and maelstrom and its impact on chromatin state and gene expression. *Cell* 151: 964–980
- Sienski G, Batki J, Senti KA, Donertas D, Tirian L, Meixner K, Brennecke J (2015) Silencio/CG9754 connects the Piwi-piRNA complex to the cellular heterochromatin machinery. *Genes Dev* 29: 2258–2271
- Stutz F, Izaurralde E (2003) The interplay of nuclear mRNP assembly, mRNA surveillance and export. *Trends Cell Biol* 13: 319–327

- Sumiyoshi T, Sato K, Yamamoto H, Iwasaki YW, Siomi H, Siomi MC (2016) Loss of I(3)mbt leads to acquisition of the ping-pong cycle in *Drosophila* ovarian somatic cells. *Genes Dev* 30: 1617–1622
- Trapnell C, Pachter L, Salzberg SL (2009) TopHat: discovering splice junctions with RNA-Seq. *Bioinformatics* 25: 1105–1111
- Uren PJ, Bahrami-Samani E, Burns SC, Qiao M, Karginov FV, Hodges E, Hannon GJ, Sanford JR, Penalva LO, Smith AD (2012) Site identification in high-throughput RNA-protein interaction data. *Bioinformatics* 28: 3013–3020
- Van Nostrand EL, Pratt GA, Shishkin AA, Gelboin-Burkhart C, Fang MY, Sundararaman B, Blue SM, Nguyen TB, Surka C, Elkins K et al (2016) Robust transcriptome-wide discovery of RNA-binding protein binding sites with enhanced CLIP (eCLIP). *Nat Methods* 13: 508–514
- Van Oss SB, Cucinotta CE, Arndt KM (2017) Emerging insights into the roles of the Paf1 complex in gene regulation. *Trends Biochem Sci* 42: 788–798
- Viphakone N, Hautbergue GM, Walsh M, Chang CT, Holland A, Folco EG, Reed R, Wilson SA (2012) TREX exposes the RNA-binding domain of Nxf1 to enable mRNA export. *Nat Commun* 3: 1006
- Vos SM, Farnung L, Boehning M, Wigge C, Linden A, Urlaub H, Cramer P (2018) Structure of activated transcription complex Pol II-DSIF-PAF-SPT6. *Nature* 560: 607–612
- Vourekas A, Zheng K, Fu Q, Maragkakis M, Alexiou P, Ma J, Pillai RS, Mourelatos Z, Wang PJ (2015) The RNA helicase MOV10L1 binds piRNA precursors to initiate piRNA processing. *Genes Dev* 29: 617–629
- Wang SH, Elgin SC (2011) *Drosophila* Piwi functions downstream of piRNA production mediating a chromatin-based transposon silencing mechanism in female germ line. *Proc Natl Acad Sci USA* 108: 21164–21169
- Wickramasinghe VO, Laskey RA (2015) Control of mammalian gene expression by selective mRNA export. *Nat Rev Mol Cell Biol* 16: 431–442
- Wiegand HL, Coburn GA, Zeng Y, Kang Y, Bogerd HP, Cullen BR (2002) Formation of Tap/NXT1 heterodimers activates Tap-dependent nuclear mRNA export by enhancing recruitment to nuclear pore complexes. *Mol Cell Biol* 22: 245–256
- Wilkie GS, Zimyanin V, Kirby R, Korey C, Francis-Lang H, Van Vactor D, Davis I (2001) Small bristles, the *Drosophila* ortholog of NXF-1, is essential for mRNA export throughout development. *RNA* 7: 1781–1792
- Yashiro R, Murota Y, Nishida KM, Yamashiro H, Fujii K, Ogai A, Yamanaka S, Negishi L, Siomi H, Siomi MC (2018) Piwi nuclear localization and its regulatory mechanism in *Drosophila* ovarian somatic cells. *Cell Rep* 23: 3647–3657
- Yu Y, Gu J, Jin Y, Luo Y, Preall JB, Ma J, Czech B, Hannon GJ (2015) Panoramix enforces piRNA-dependent cotranscriptional silencing. *Science* 350: 339–342
- Zhang Y, Liu T, Meyer CA, Eeckhoute J, Johnson DS, Bernstein BE, Nusbaum C, Myers RM, Brown M, Li W et al (2008) Model-based analysis of ChIP-Seq (MACS). *Genome Biol* 9: R137
- Zhang F, Wang J, Xu J, Zhang Z, Koppetsch BS, Schultz N, Vreven T, Meignin C, Davis I, Zamore PD et al (2012) UAP56 couples piRNA clusters to the perinuclear transposon silencing machinery. *Cell* 151: 871–884
- Zhao K, Cheng S, Miao N, Xu P, Lu X, Zhang Y, Wang M, Ouyang X, Yuan X, Liu W et al (2019) A Pandas complex adapted for piRNA-guided transposon silencing. *bioRxiv* <https://doi.org/10.1101/608273> [PREPRINT]